New Phytologist

Research

Intermolecular base-pairing interactions, a unique topology and exoribonuclease-resistant noncoding RNAs drive formation of viral chimeric RNAs in plants

Katalin Nemes[1], Jose F. Gil[1,2], Sebastian Liebe[3], Mansi Mansi[1], Efstratia Poimenopoulou[1], Britt-Louise Lennefors[4], Mark Varrelmann[3] and Eugene I. Savenkov[1]

[1]Department of Plant Biology, Linnean Center for Plant Biology, Swedish University of Agricultural Sciences (SLU), Uppsala, 75007, Sweden; [2]VEDAS Corporación de Investigación e Innovación (VEDAS CII), Medellín, 050024, Colombia; [3]Department of Phytopathology, Institute of Sugar Beet Research, Göttingen, 37079, Germany; [4]Department of Plant Pathology, DLF Beet Seed AB, Landskrona, 261 91, Sweden

Author for correspondence:
Eugene I. Savenkov
Email: eugene.savenkov@slu.se

Received: *4 May 2023*
Accepted: *2 October 2023*

New Phytologist (2024) **241:** 861–877
doi: 10.1111/nph.19346

Key words: 5′→3′ exoribonuclease, benyvirus, exoribonuclease-resistant RNAs, RNA virus, XRN4.

Summary

- In plants, exoribonuclease-resistant RNAs (xrRNAs) are produced by many viruses. Whereas xrRNAs contribute to the pathogenicity of these viruses, the role of xrRNAs in the virus infectious cycle remains elusive.
- Here, we show that xrRNAs produced by a benyvirus (a multipartite RNA virus with four genomic segments) in plants are involved in the formation of monocistronic coat protein (CP)-encoding chimeric RNAs. Naturally occurring chimeric RNAs, we discovered, are composed of 5′-end of RNA 2 and 3′-end of either RNA 3 or RNA 4 bearing conservative exoribonuclease-resistant 'coremin' region.
- Using computational tools and site-directed mutagenesis, we show that *de novo* formation of chimeric RNAs requires intermolecular base-pairing interaction between 'coremin' and 3′-proximal part of the CP gene of RNA 2 as well as a stem-loop structure immediately adjacent to the CP gene. Moreover, knockdown of the expression of the *XRN4* gene, encoding 5′→3′ exoribonuclease, inhibits biogenesis of both xrRNAs and chimeric RNAs.
- Our findings suggest a novel mechanism involving a unique tropology of the intermolecular base-pairing complex between xrRNAs and RNA2 to promote formation of chimeric RNAs in plants. XrRNAs, essential for chimeric RNA biogenesis, are generated through the action of cytoplasmic Xrn 4 5′→3′ exoribonuclease conserved in all plant species.

Introduction

Most cellular and viral RNAs fold into distinctive and complex 3D structures that are essential for various biological processes. The inherent property of RNA as flexible and dynamic molecule makes it an ideal platform for alteration of 3D structure in response to diverse cellular conditions (Ganser *et al.*, 2019). Many RNA viruses actively explore this property to regulate expression of their genomes, to suppress host defence mechanisms, and even to co-opt cellular RNA decay machinery to produce exoribonuclease-resistant RNAs (xrRNAs; Pijlman *et al.*, 2008; Moon *et al.*, 2012; Peltier *et al.*, 2012; Schuessler *et al.*, 2012; Schnettler *et al.*, 2012; Bidet *et al.*, 2014; Liu *et al.*, 2014; Roby *et al.*, 2014; Manokaran *et al.*, 2015; Moon *et al.*, 2015a,b; Akiyama *et al.*, 2016; Flobinus *et al.*, 2016; Charley *et al.*, 2018; Steckelberg *et al.*, 2018a,b). Moreover, viral RNAs can be engaged in various intramolecular and intermolecular base-pairing interaction leading to template switching during virus replication cycles and, subsequently, formation of various aberrant and defective RNAs (D-RNAs), among which defective interfering RNAs (DI-RNAs) are the most well studied class of these molecules (Pathak & Nagy, 2009; Lukhovitskaya *et al.*, 2013).

Beet soilborne mosaic virus (BSBMV) and beet necrotic yellow vein virus (BNYVV), both positive-sense single-stranded RNA (+ssRNA) viruses, belong to the genus *Benyvirus* (family Benyviridae). The BSBMV has four-partite genome, whereas BNYVV has four- or five-partite genome depending on the virus isolate with RNA 5 as an additional genomic component (Koenig *et al.*, 1997). Following cell entry, the genome is translated into six proteins in addition to the synthesis of subgenomic RNAs (sgRNAs) that encode another four to six accessory proteins (Niehl *et al.*, 2021). Collectively, these proteins enable viral replication, cell-to-cell movement, assembly, and transmission in soil by a plasmodiophorid vector *Polymyxa betae* (Niehl *et al.*, 2021).

Both viruses have similar genome organisation (Niehl *et al.*, 2021). High levels of sequence conservation and sequence identity between BSBMV and BNYVV suggest functional similarity of the corresponding genes in both viruses. Furthermore, the genomic components can be exchanged between two viruses

resulting in viable reassortants (Lee *et al.*, 2001; Ratti *et al.*, 2009; Gil *et al.*, 2018). The RNA1 encodes a viral replicase harbouring motifs for methyltransferase, helicase, papain-like protease and RNA-dependent RNA polymerase. The RNA2 encodes a coat protein (CP), a longer version of CP with a readthrough domain (CP-RTD) involved in vector transmission, the triple gene block (TGB) of movement proteins and a zinc-finger protein (P14), a viral suppressor of RNA silencing (Tamada & Kusume, 1991; Gilmer *et al.*, 1992; Chiba *et al.*, 2013). The BNYVV RNA3 is needed for long-distance movement of the virus in *Beta* species (Lauber *et al.*, 1998) and encodes the P25 virulence factor responsible for development of rhizomania syndrome in sugar beet (Tamada *et al.*, 1999). Likewise, BSBMV RNA3 is also involved in long-distance movement of the virus, but encodes a 29 kDa protein (P29) that shares only a 23% amino acid sequence identity with the P25 virulence factor (Ratti *et al.*, 2009). The P31 and P32 proteins encoded by RNA4 of BNYVV and BSBMV, respectively, are required for efficient transmission of the viruses by *P. betae* vector (Tamada & Abe, 1989; D'Alonzo *et al.*, 2012).

Several types of D-RNAs and DI-RNAs associated with benyvirus infections (Wang *et al.*, 2011). Moreover, BNYVV RNA 3 employs structures located in its 3′-untranslated region (UTR) to stall 5′→3′ exoribonuclease (Xrn; Flobinus *et al.*, 2018). This process results in the production of xrRNA or so-called noncoding RNA 3 (ncRNA3) that participates (together with the P14 protein) in suppression of RNA silencing, the host antiviral defence mechanism (Flobinus *et al.*, 2016). The studies of 'core' sequence providing Xrn resistance led to identification of the 20 nt-long 'coremin' motif conserved in all benyviruses and some cucumoviruses (Peltier *et al.*, 2012). ncRNA3 achieves Xrn1 resistance through formation of two proximal hairpins separated by a short spacer sequence (Dilweg *et al.*, 2019).

D'Alonzo *et al.* (2012) described accumulation of noncoding aberrant (chimeric) RNA consisting of partial sequences of RNA 3 and RNA 4 of BNYVV. Although, nothing is known about biogenesis of this particular RNA or whether it is produced *de novo* during virus replication cycles, the aberrant RNA remained stable even after 20 serial manual passage of the virus in *Chenopodium quinoa* (D'Alonzo *et al.*, 2012). Furthermore, in other viruses, some novel types of RNAs have been reported, including tandem duplications of 3′-termini and even generation of dimeric viral RNA species (Bertran *et al.*, 2016; Blum *et al.*, 2017). Noticeably, in both cases the duplications were arranged in a head-to-tail array. The molecular mechanism hypothesised to give rise to such molecules relies on the assumption that, during replication, template switching occurs presumably on intermolecular base-pairing complexes. Indeed, *in silico* analysis showed that intermolecular base-pairing interaction could be widespread and common among multipartite RNA viruses (Gilmer *et al.*, 2018).

These discoveries suggest that the network of base-pairing interactions in viruses can be more complex than previously anticipated. Moreover, upon virus replication, these interactions might give rise to novel, yet uncharacterised or overlooked RNA species. Indeed, in this study, we report a discovery of novel monocistronic CP-encoding chimeric RNA species associated with benyvirus infections. Our work revealed three principal features – namely: a stem-loop (SL) region immediately adjacent to the CP cistron of RNA 2; a intermolecular base-pairing region formed between 3′-proximal part of the CP cistron of RNA2 and the 'coremin' region of RNA 3 or RNA 4; and xrRNAs – regulating formation of chRNAs. We also identified 'coremin' sequence conserved in many viruses as a pivotal element controlling biogenesis of chRNAs. Remarkably, our data also provide evidence for dual role of 'coremin' in virus infection cycle: first as a folded RNA motif that blocks processive Xrn and second as an element involved in intramolecular base-pairing with the genomic RNA2 leading to chRNA formation through template switching during virus replication. Our results suggest an additional level of organisation and expression of viral RNA genomes – formation of functional chRNAs – beyond classical genomic and sgRNA species.

Materials and Methods

Sample material and RNA isolation

Sugar beet (*Beta vulgaris* L. ssp. *vulgaris*) plants were sown and kept in a quarantine glasshouse at DLF Beet Seed AB (Landskrona, Sweden). One-week-old plants were transferred to 0.5 l pots supplied with sieved soils containing resting spores of *Polymyxa betae* carrying BSBMV (BSBMV-infested soil).

Nicotiana benthamiana Domin and *Beta vulgaris* L. ssp. *macrocarpa* (Guss.) Thell. plants were grown under long-day conditions (16 h : 8 h, light : dark) with minimum daytime temperature of 22°C and night-time temperature of 18°C. Four-week-old *N. benthamiana* and *B. vulgaris* ssp. *macrocarpa* plants were used for agroinoculation of BSBMV infectious clones (Laufer *et al.*, 2018) and chimeric RNA clones.

For RNA extraction, root (sugar beet) and leaf samples (*N. benthamiana* and *B. vulgaris* ssp. *macrocarpa*) were collected 4 wk after inoculation. Total RNA was extracted using the MagJET RNA Purification Kit (Thermo Fisher Scientific, Uppsala, Sweden) according to the manufacturer's instructions, including DNase treatment.

Northern blot analysis

For Northern blot analysis, 3 μg of total RNA preparations was separated by formaldehyde gel electrophoresis, transferred to nylon membranes (Hybond-N; Amersham Biosciences, Buckinghamshire, UK), cross-linked and hybridised as described (Sambrook *et al.*, 1989). Antisense random-primed Digoxigenin-dUTP-labelled (Sigma-Aldrich) RNA3 3′-UTR- and RNA4 3′-UTR-specific RNA probes were synthesised with T7 RNA polymerase (Promega).

Construction of plasmids

Standard recombinant DNA procedures were followed by use of a combination of PCR, site-directed mutagenesis and 'Gibson assembly' (Gibson *et al.*, 2009). For cloning purposes, RT reactions were performed using Superscript III reverse transcriptase

(Thermo Fisher Scientific) supplemented with 1× RT reaction buffer (50 mM Tris–HCl pH 8.3, 75 mM KCl, 3 mM MgCl2, 1 mM DTT), 2.5 μM reverse primer, 0.5 mM dNTPs and 1 U RiboLock RNase inhibitor (Thermo Fisher Scientific). Full-length cDNAs of BSBMV RNA components were PCR amplified with Phusion High-Fidelity DNA Polymerase (Thermo Fisher Scientific). Two additional PCR products (2.0 and 1.2 kb) were cloned into a binary vector pCB302 (KX510272.1) using In-fusion HD Cloning Kit (Takara Bio Inc., Kyoto, Japan) following the instructions of the manufacturer. The forward and reverse primers (Supporting Information Table S1) were designed to generate PCR products containing 5′-ends with 20 bp of sequence identity to the linearised pCB302 vector. The vector was linearised using 35S-pCB and HDV-pCB primers. The amplified PCR products and the amplified linearised vector (opened pCB302) were spin-column purified before an In-fusion-HD cloning reaction. The reactions were then transformed into Stellar competent cells (Takara Bio Inc.). The purified plasmids were verified with restriction digestion followed by sequencing (Macrogen Europe, Amsterdam, the Netherlands).

To obtain R2R3-BNCP, R2R4-BNCP, R2R3-mRFP and R2R4-mRFP constructs, BNYVV CP and mRFP genes were amplified with specific primers (Table S1) and cloned into pCB302-R2R3 and pCB302-R2R4 full-length infectious agroclones engendered previously (see a paragraph above). To this end, pCB302-R2R3 and pCB302-R2R were PCR-opened using specific primers (Table S1) and recombined with corresponding BNYVV CP and mRFP PCR products using In-fusion HD Cloning Kit, replacing BSBMV CP gene, respectively.

To obtain No-SL1, No-cor-inter, R3-flop-coremin and R4-flop-coremin constructs, a PCR-based mutagenesis was employed using infectious full-length R2R3 and R2R4 clones (pCB302-R2R3 and pCB302-R2R4 plasmids) as a backbone. Specific primers introducing point mutations are listed in Table S1. PCR products with introduced mutations were recombined into pCB302-R2R3 and pCB302-R2R4 plasmids using In-fusion HD Cloning Kit replacing wt sequences. In the R3-flop-coremin and R4-flop-coremin constructs, the 'coremin' region was replaced with its reverse complement sequence.

In vitro transcription

Templates for *in vitro* transcription were generated by PCRs performed on infectious full-length cDNA clones of BSBMV (Laufer *et al.*, 2018) using specific primers (Table S1). *In vitro* transcripts of BSBMV RNA2, RNA3 and RNA4 were produced with the T7 RiboMAX™ Express Large Scale RNA Production System (Promega) according to the manufacturer's instructions. Transcripts were gel purified with the NucleoSpin Gel and PCR Clean-up (Macherey-Nagel) according to the manufacturer's instructions. Purified transcripts were quantified in a NanoDrop (DeNovix, Wilmington, DE, USA). Each RNA (100 ng) was subjected to cDNA synthesis alone and in a mixture with all RNAs using SuperScript III Reverse Transcriptase (Invitrogen). Potential chimeric RNAs were detected with specific primers using Phusion™ High-Fidelity DNA Polymerase (Thermo Fisher Scientific).

RT-PCR and analysis of stability of introduced mutations

One-microgram aliquots of total RNA samples were used for oligo(dT)-primed cDNA synthesis with Superscript III reverse transcriptase (Thermo Fisher Scientific). The obtained cDNAs were used as templates for a PCR with Phusion High-Fidelity DNA Polymerase (Thermo Fisher Scientific) and BSBMV-specific primers, or gene-specific primers (*NbEF1α*), or BSBMV-specific plus poly(T) primer (chimeric RNA detection).

The stability of the introduced mutations (see above) was verified with RT-PCR using the primers detailed in Table S1. The amplified PCR product was purified using the GeneJET PCR Purification Kit (Thermo Fisher Scientific) and sequenced (Macrogen).

Quantification of BSBMV genomic and chimeric RNAs by RT-qPCR

For qPCR, iScript cDNA synthesis kit (Bio-Rad) was used according to the manufacturer's instructions, followed by qPCR using DyNAmo Flash SYBR Green qPCR Kit (Thermo Fisher Scientific). One-microgram aliquots of total RNA were used for cDNA synthesis in all cases. For quantification of BSBMV genomic and chimeric RNA, an absolute quantification by RT-qPCR was performed by using plasmids containing each of the BSBMV genomic RNA components and/or chimeric RNAs (R2R3 and R2R4, respectively) for standard curve estimation (10-fold serial dilution starting from 100 pg μl^{-1} to 1 fg μl^{-1}). The total copy number was estimated using the formula: copy number = (ng × 6.0221 × 10^{23})/(length × 660 × 1 × 10^{9}) (Olmos *et al.*, 2005). Primers used for RT-qPCRs are given in Table S1. At least three biological replicates were used in the experiments with three technical replicates per each biological replicate.

Analysis of RNA-Seq data

BSBMV RNA-Seq data were published previously (Gil *et al.*, 2020). Reads that did not map to the sugar beet genome were used to identify the presence of the reads corresponding to chimeric RNAs. These reads were mapped against BSBMV genome and chimeric RNA sequences using BOWTIE2. Files were sorted and duplicates were removed using SAMTOOLS. The files were then indexed and visualised in IGV software (Integrative Genomic Viewer http://software.broadinstitute.org/software/igv). Reads spanning the junction site of the chimeric RNAs were extracted using SAMTOOLS. Reads mapping to the chimeric RNAs were plotted in R.

Agroinoculation

Agroinoculation of *N. benthamiana* and *B. vulgaris* ssp. *macrocarpa* leaves was conducted by pressure infiltration as described previously (Laufer *et al.*, 2018). *Agrobacterium tumefaciens* strains delivering the full-length infectious cDNA clones of BSBMV genomic RNAs, chimeric RNAs and their mutant derivatives were adjusted to an OD_{600} of 0.5 each, mixed in desired combinations and infiltrated onto leaves using a syringe without a needle.

ELISA

A double antibody sandwich enzyme-linked immunosorbent assay (DAS-ELISA) was conducted to analyse the virus content of BNYVV and BSBMV in leaf tissue of *N. benthamiana* (100–150 mg). Antibodies specific for BNYVV CP (AS-0737) or BSBMV CP (RT-1035) were obtained from the Leibniz Institute DSMZ-German Collection of Microorganisms and Cell Cultures (Braunschweig, Germany). The Precellys 24 tissue homogeniser (Bertin Instruments) was used to grind the leaf material in sample buffer (1 : 20, w/v) for 45 s at 1400 ***g***. The ELISA was conducted according to the manufacturer's instructions. Raw absorbance values measured at 405 nm were corrected by subtraction of blank and buffer control.

Modelling of RNA structures

RNA structural elements were modelled using Mfold (http://www.unafold.org/mfold/applications/rna-folding-form-v2.php; Zuker, 2003), pKiss (https://bibiserv.cebitec.uni-bielefeld.de/pkiss; Janssen & Giegerich, 2015) and CentroidFold (http://rtools.cbrc.jp/centroidfold/; Sato *et al.*, 2009), using default parameters. RNA structures were visualised using RNA structures drawing program (https://rna2drawer.app/; Johnson *et al.*, 2019).

RNA quantification in *N. benthamiana* plants inoculated with the mutant derivatives of RNA3 and RNA4

Total RNA was extracted from 100 mg of leaf tissue as described previously (Onate-Sanchez & Vicente-Carbajosa, 2008). One microgram of total RNA was used for the reverse transcription with iScript cDNA Synthesis Kit according to the manufacturer's instruction (Bio-Rad). The cDNA samples were diluted 10 times and 4 µl aliquots were used as a template for qPCR. Accumulation of both chimeric RNAs and coremin-depleted chimeric RNAs was measured by RT-qPCR as described above. Primers used for RT-qPCR quantification of chimeric RNAs are given in Table S1. At least three biological replicates were used in the experiments with three technical replicates per each biological replicate.

xrRNA quantification

Stem-loop reverse transcription primers were designed as described previously (Kalyandurg *et al.*, 2019). To quantify the accumulation of minus strand of the xrRNAs, 1 µg of isolated total RNA was used for SL RT using RevertAid Reverse Transcriptase (Thermo Fisher Scientific) with SL RT primer and *NbPP2A* reference gene reverse primer (Table S1) according to the manufacturer's instructions. Real-time PCR was performed using Dynamo Flash SYBR Green (Thermo Fisher Scientific). The C_t values of noncoding RNA accumulation were normalised to the C_t values of the *NbPP2A* reference gene.

For direct quantification of xrRNA accumulation, SL qPCR was performed on reverse-transcribed RNAs. One microgram of total RNA preparations was reverse transcribed using SuperScript™ IV Reverse Transcriptase (Thermo Fisher Scientific) and oligo(dT) primer followed by an RNAse H treatment (Thermo Fisher Scientific). The cDNA was extracted with TRIzol® (Thermo Fisher Scientific) regent and washed with ethanol according to the manufacturer's instructions. The cDNAs were annealed with the SL RT primer followed by filling in the 5′ overhangs using Klenow Fragment (Thermo Fisher Scientific). The RT-qPCR was performed as described above.

Virus-induced gene silencing

To obtain TRV:*Xrn4* silencing construct, a 600-bp fragment of *NbXRN4* (Accession no. KY402212.1) was amplified by PCR using cDNA as a template and cloned in an antisense orientation into tobacco rattle virus (TRV) construct pTRV:00 (Liu *et al.*, 2002) digested with *Xho*I and *Eco*RI. The resulting construct was transformed into *A. tumefaciens* strain C58C1. *N. benthamiana* plants were co-infiltrated with TRV RNA1 construct pTRV1. Agrobacterium strains delivering pTRV:00 (TRV2) were used as a control. Two weeks postinfiltration, total RNA was isolated for RT-qPCR to assess *NbXRN4* accumulation. Two weeks postinfiltration, TRV:*XRN4* and TRV:00 control plants were agroinoculated with BSBMV full-length cDNA clones on the second leaf above previously infiltrated as described above to assay BSBMV genomic RNAs, chRNAs and noncoding xrRNAs accumulation in the *NbXRN4*-silenced plants. One hundred milligram samples for RNA extraction were collected from the third leaf above inoculated 14 d postinoculation with BSBMV.

Results

Discovery, identification and characterisation of the chimeric RNAs associated with BSBMV infections in plants

An effort to engineer a full-length BSBMV RNA 2 cDNA from BSBMV-infected sugar beet roots led to amplification of a PCR product of the expected size (*c.* 4.6 kb) and two additional predominant PCR products (*c.* 2.0 and 1.2 kb), whereas RT-PCR performed to amplify a full-length RNA1 resulted only in a single PCR product of the expected size (*c.* 6.7 kb; Fig. 1a). The additional PCR products were cloned and sequenced. Sequence analysis of 20 randomly selected clones revealed that the 1.2-kb PCR fragment is heterogeneous in sequence and corresponds to three novel major classes of RNA molecules: a defective RNA encompassing the 5′-terminal 791 nucleotides (nt) and 3′-terminal 372 nt of RNA2; a chimeric RNA encompassing the 5′-terminal 721 nt of RNA 2 and 3′-terminal 486 nts of RNA 3 (referred to as R2R3; Fig. S1a); a chimeric RNA encompassing the 5′-terminal 721 nts of RNA 2 and 3′-terminal 429 nts of RNA 4 (referred to as R2R4; Fig. S1b). Thus, these novel chimeric RNAs (chRNAs) represent monocistronic CP-encoding RNAs, in which intact CP ORF is followed by a conservative 21-nt-long 'coremin' region (Figs 1b, S1).

To assess chRNA accumulation, we quantified R2R3 and R2R4 as well as genomic RNA 2, RNA 3 and RNA 4 in the roots of sugar beet plants grown in the soil infested with BSBMV.

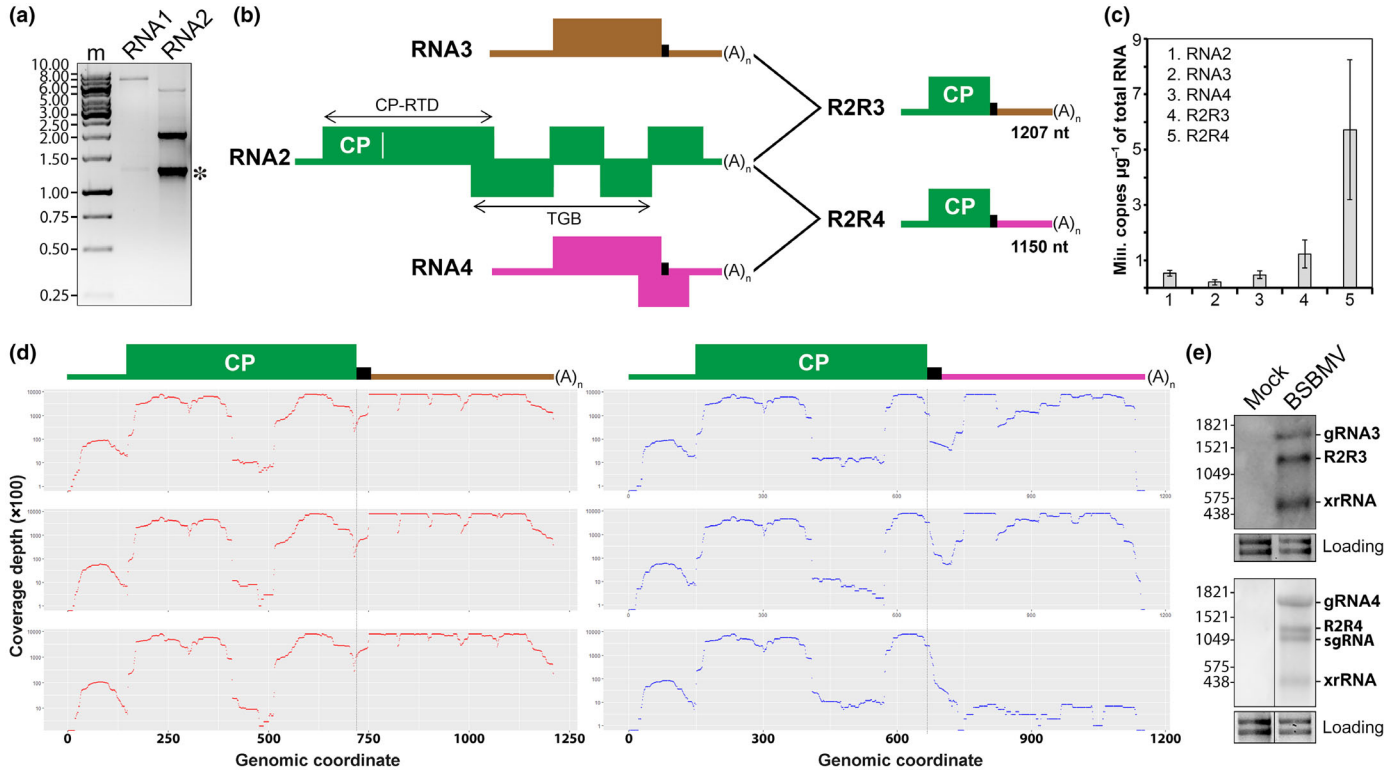

Fig. 1 Identification and characterisation of the chimeric RNAs associated with beet soilborne mosaic virus (BSBMV) infections in *Beta vulgaris* ssp. *vulgaris*. (a) RT-PCR of cDNA of sugar beet roots grown in BSBMV-infested soil to amplify full-length cDNA of RNA 1 and RNA2 using a genomic RNA-specific (forward) and poly(T) (reverse) primers. An additional amplification product corresponding to chimeric RNAs is indicated with an asterisk. The nucleotide length (in kb) of marker DNAs (m) is shown on the left. (b) Schematic of the BSBMV genomic RNAs (RNA2, RNA3 and RNA4) and the chimeric RNAs: R2R3 and R2R4. The lengths of the chimeric RNAs (1207 and 1150 nt, respectively) without poly(A) tail are indicated. Rectangles denote ORFs. Small black rectangles denote conserved 'coremin' region. (c) Quantification of the accumulation of BSBMV genomic (RNA2, RNA3 and RNA4) and chimeric RNAs by absolute RT-qPCR in roots of sugar beet plants grown in BSBMV-infested soil. Data are means ± SD; $n = 3$. (d) RNA-Seq assembly plots showing the distribution of the reads across the sequences of R2R3 (left) and R2R4 (right) schematically shown above the plots. Plots for three biological replicates for each RNA are presented. The dashed lines indicate the RNA2/RNA3 and RNA2/RNA4 junction points, respectively. (e) Northern blot analyses depicting the accumulation of chimeric and exoribonuclease-resistant (xr) RNAs in the roots sugar beet plants infected with BSBMV. The membranes were hybridised with probes complementary to the 3′-untranslated region (UTRs) of BSBMV RNA3 and RNA4, respectively. The nucleotide length of marker RNAs is shown on the left. gRNA3 and gRNA4, genomic RNA3 and RNA4, respectively. sgRNA, putative subgenomic RNA. $(A)_n$, poly A tail.

RT-qPCR data showed that the chRNAs accumulate at levels higher than those of the genomic RNA2, RNA3 and RNA4 (Fig. 1c). To resolve whether chRNAs are borne *de novo* during virus replication cycles, as an inoculum, we employed full-length infectious cDNA clones of BSBMV (RNA 1 + RNA 2 + RNA 3 + RNA 4) that did not contain chimeric RNAs. To monitor chRNA emergence, we assessed R2R3 and R2R4 accumulation in upper systemically infected leaves of *Beta vulgaris* ssp. *macrocarpa* and *Nicotiana benthamiana* plants inoculated with the infectious cDNA clones of BSBMV. Quantification of RNA 2, R2R3 and R2R4 at 28 d postinoculation (dpi) showed that, in these two hosts, the chRNAs accumulated at the total levels (R2R3 + R2R4) higher than those of the reference genomic RNA2, although the levels of R2R3 were higher in *Beta vulgaris* ssp. *macrocarpa*, whereas R2R4 accumulated higher in *N. benthamiana*, suggesting dependence of the accumulation on the host (Fig. S2). Thus, we concluded that chRNAs are generated *de novo* during virus infection process and can be readily detectable in upper systemically infected leaves.

We sought to test whether chRNAs could be artefacts of RT-PCR amplification and whether the production of chRNAs requires virus replication. To this end, RT-PCRs were performed on full-length *in vitro* generated BSBMV transcripts, on RNA transcripts supplemented with xrRNAs transcripts and on total RNA isolated from leaves infiltrated with BSBMV full-length infectious cDNA clones in the absence of RNA 1 (which provides a replication function). The results revealed a lack of chRNA production (Fig. S3). Therefore, we concluded that the biogenesis of chRNAs requires virus replication and that chRNAs are not artefacts of RT-PCR amplification.

We subsequently profiled the transcriptomes (RNA-Seq) of sugar beet roots infected with BSBMV (Gil *et al.*, 2018) and identified reads spanning the RNA2/RNA3 and RNA2/RNA4 junction sites of the chRNAs (Fig. 1d). Additionally, this analysis revealed some heterogeneity at the junction site characterised by slightly different number of nts between CP ORF and 'coremin', but this variability did not affect overall structure of chRNAs (Fig. S4).

Additionally, the emergence of chRNAs was monitored by northern blot analysis of RNA from systemically infected leaves of *N. benthamiana* with probes targeting the viral 3′UTR of either RNA 3 or RNA 4 (Fig. 1e). Besides full-length genomic RNA 3 and RNA 4, in each case, additional faster-migrating molecules could be detected. The sizes of these molecules corresponded to the expected sizes of R2R3 (1207 nts), R2R4 (1150 nts), a putative sgRNA (probably for the expression of the second ORF of RNA4) and corresponding xrRNAs (predicted sizes are of 485 and 427 nt, respectively; Fig. 1e).

Chimeric RNAs can move systemically and can be translated to yield CP

Having determined that chRNAs are produced during BSBMV replication cycles, we set up experiments to evaluate whether these peculiar RNAs are biologically active. To this end, we took advantage of two characteristic properties of BSBMV: the ability of BSBMV RNA 1 + RNA 2 to move systemically in *N. benthamiana* plants (Gil *et al.*, 2018; Laufer *et al.*, 2018) in the absence of RNA 3 and RNA 4; and high similarity between BSBMV and BNYYV genomic components, which can be exchanged between the viruses as they can be *trans*-replicated and *trans*-encapsidated (heterologous encapsidation; Gil *et al.*, 2018; Laufer *et al.*, 2018).

To address the question of whether chRNAs can move from the inoculated to the upper leaves in the presence of RNA 1 and RNA 2, which provide the replication and movement functions, as well as CP and CP-RTD encoded directly by RNA2, respectively, three inocula were assembled comprising RNA1 + RNA2 (BS12 control inoculum), RNA 1 + RNA 2 + R2R3 (BS12 + R2R3), and RNA 1 + RNA 2 + R2R4 (BS12 + R2R4) and inoculated on leaves of *N. benthamiana* plants. Since RNA 3 is required for BSBMV systemic movement in *B. vulgaris* ssp. *macrocarpa* plants, three additional inocula were assembled comprising RNA1 + RNA2 + RNA3 (BS123 control inoculum), RNA 1 + RNA 2 + RNA 3 + R2R3 (BS123 + R2R3) and RNA 1 + RNA 2 + RNA 3 + R2R4 (BS123 + R2R4) and inoculated on leaves of *B. vulgaris* ssp. *macrocarpa* plants. Compared with BS12-infected *N. benthamiana* plants, which showed typical viral symptoms (Fig. 2a), plants systemically infected with BS12 + R2R3 or BS12 + R2R3 exhibited slightly more severe symptoms (Fig. 2a), whereas there was not much difference in the symptoms appearance in *B. vulgaris* ssp. *macrocarpa* infected leaves characterised by mild chlorosis and leaf malformation 21 dpi (Fig. 2b). At 21 dpi, RT-qPCR data determined accumulation of both R2R3 and R2R4 in upper systemically infected leaves (Fig. 2c). The results show that chRNAs are fully competent in replication and long-distance movement even when they are not produced *de novo* (since RNA 3 and RNA 4 were absent from the inoculum for *N. benthamiana*, and RNA 4, but not RNA 3, was absent from the inoculum for *B. vulgaris* ssp. *macrocarpa*).

To determine whether CP is translated from chRNAs we performed infection experiments with recombinant viruses, in which CP ORF in the BSBMV chRNAs was replaced with that of BNYVV (R2R3-BN-CP and R2R4-BN-CP constructs, respectively). To inoculate the leaves of *N. benthamiana* plants, five different inocula were assembled, each comprising BSBMV RNA 1 + RNA 2, and chRNAs (R2R3 or R2R4, respectively) or their recombinant BNYVV derivatives (R2R3-BN-CP or R2R4-BN-CP, respectively). Foliar symptoms on *N. benthamiana* plants produce by these five inocula in the upper leaves were similar, with typical development of yellow mosaic and leaf malformations (Fig. 2d). The ELISAs performed on extracts prepared from upper leaves of the infected plants 21 dpi clearly showed that BNYVV CP translated from chRNAs could be readily detected (Fig. 2e). Moreover, when CP ORF in chRNAs was replaced with a gene for red fluorescent protein (mRFP), red fluorescent infection loci could be readily detectable by microscopy in the inoculated leaves (Fig. S5). However, the mRFP constructs did not move systemically as no mRFP fluorescence was detected in upper systemically infected leaves. These data support the notion that chRNAs with the intact CP gene are transported systemically, whereas the virus does not support systemic movement of chRNAs in which CP gene is replaced with 'foreign' mRFP suggesting that the sequence of CP ORF might be *cis*-acting and important for the systemic movement of CP-encoding RNAs (RNA 2 and chRNAs), the phenomenon requires further investigation, but is beyond the scope of this paper.

The role of RNA structural elements in chRNA biogenesis

Since both BSBMV and BNYVV share identical 'coremin' sequence, next we sought to explore whether chRNA production accompanies infections established from the inoculum in which genomic RNA 3 of BSBMV is replaced with that of BNYVV. To

Fig. 2 Chimeric RNAs can move from lower inoculated leaves to upper noninoculated systemically infected leaves of *Nicotiana benthamiana* and *Beta vulgaris* ssp. *macrocarpa*, and coat protein (CP) translated from chimeric RNAs is incorporated into virus particles. (a) Appearance of the symptoms induced by beet soilborne mosaic virus (BSBMV) RNA1 + RNA2 (BS12) and by BS12 supplemented with chimeric RNAs in *N. benthamiana* 21 dpi. (b) Foliar symptoms on *B. vulgaris* ssp. *macrocarpa* produced by BSBMV RNA1 + RNA2 + RNA3 (BS123) and by BS123 supplemented with chimeric RNAs in upper leaves 21 dpi. (c) Quantification of the accumulation of BSBMV genomic (RNA2) and chimeric RNAs by absolute RT-qPCR in the systemically infected leaves of *N. benthamiana* and *B. vulgaris* ssp. *macrocarpa*. Data are means ± SD; $n = 3$. Type of the inoculum is indicated below the graph. Notice that inoculum for *B. vulgaris* ssp. *macrocarpa* was supplemented with RNA 3 for efficient virus movement in this particular host. (d) Appearance of the symptoms induced by BS12 and BS12 supplemented with chimeric RNAs and their derivatives on the fifth leaf above inoculated 21 dpi. (e) Detection of BSBMV and beet necrotic yellow vein virus (BNYVV) CP antigens by enzyme-linked immunosorbent assay (ELISA) as indicated by absorbance values at 405 nm. Plant extracts were prepared from upper systemically infected leaves at 21 dpi. Type of the inoculum is indicated below the graph. BS12, BSBMV RNA1 + RNA2. Note that BNYVV and BSBMV ELISA data were plotted on the same graph for better visualisation, but not for comparison between BNYVV and BSBMV. Data are means ± SD; $n = 3$. dpi, days postinoculation.

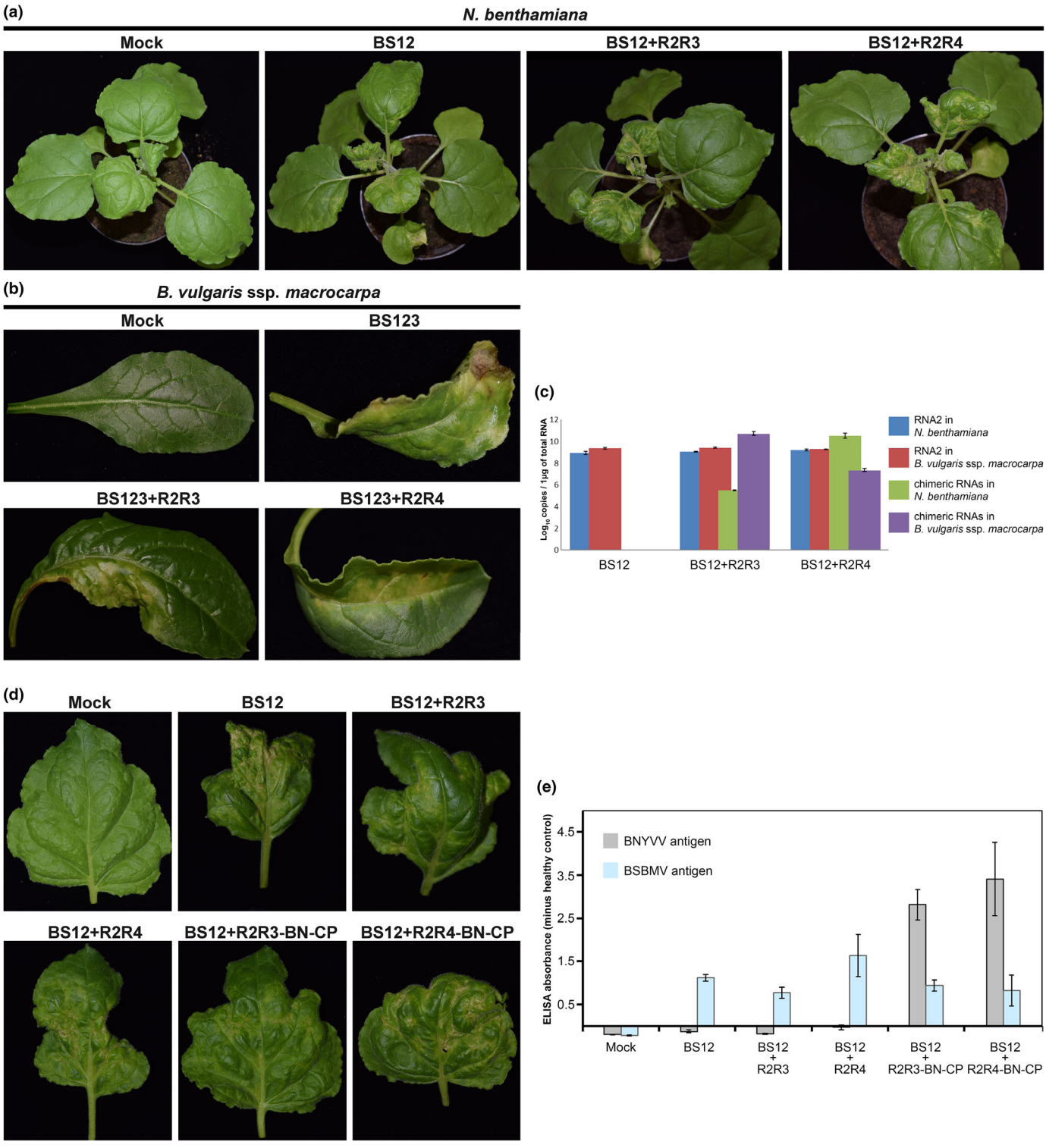

this end, RNA 1 and RNA 2 of BSBMV were co-inoculated with BNYVV RNA 3 on the leaves of *B. vulgaris* ssp. *macrocarpa* plants. Twenty-one days postinoculation RT-PCR amplification, cloning and sequencing revealed a chRNA that was similar in structure to the previously characterised BSBMV R2R3 (Fig. S6). As expected, this particular chRNA encompassed the 5′-terminal 724 nt of BSBMV RNA 2 and 3′-terminal 545 nts of BNYVV RNA 3 including 'coremin' (Fig. S6).

Given the results above as well as the presence of 'coremin' in all chRNAs we discovered in this study, we reasoned that 'coremin' is absolutely essential for chRNA biogenesis. Therefore, we hypothesised that base-pairing interactions between RNA 2 and

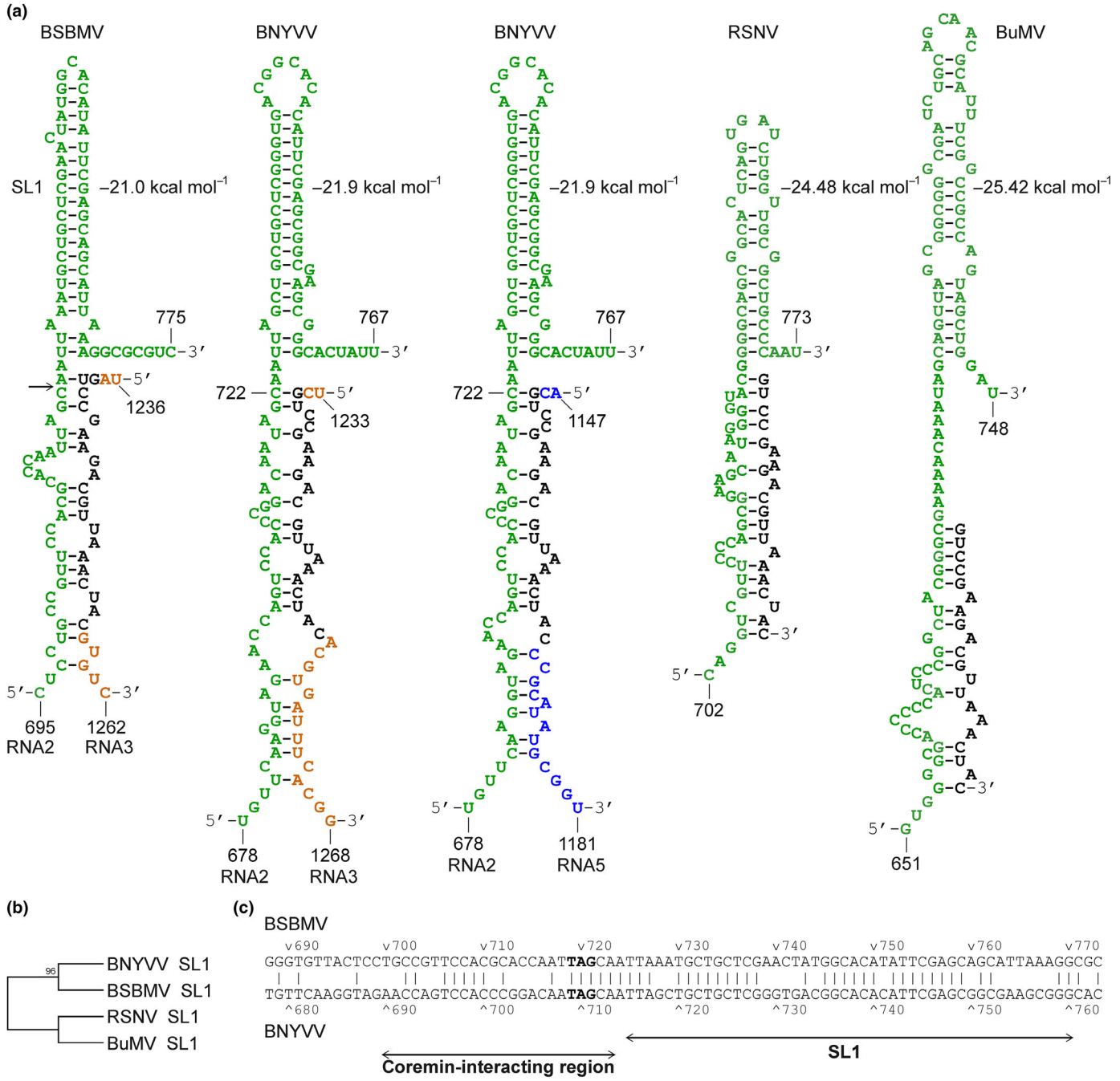

Fig. 3 Models of the secondary structure of SL1 and the intermolecular base-pairing complex with 'coremin'. (a) Predicted stem-loop structure (SL1) in RNA2 of benyviruses, and predicted base-pairing interaction between RNA 2 and 'coremin'. Numbering refers to nucleotide positions in the plus strand of full-length genomic RNAs of various benyviruses. 'Coremin' sequence is shown in black script. RNA2 sequence is shown in bold green script, whereas RNA3 of both beet soilborne mosaic virus (BSBMV) and beet necrotic yellow vein virus (BNYVV), and RNA5 of BNYVV sequences are shown in brown and in blue scripts, respectively. Arrowhead indicates junction site in chimeric RNAs. (b) A phylogenetic tree inferred by the neighbour-joining (NJ) method from multiple sequence alignments of the isolated SL1 sequences. The percentages (> 70%) of replicate trees in which the associated sequences clustered together in the bootstrap test (3000 replicates) are shown next to the branches. (c) Sequence alignment of BSBMV and BNYVV RNA2 fragments annotated to show the boundaries of predicted structural elements. Nucleotides are numbered at 10-nucleotide intervals, and the termination codons of the BSBMV and BNYVV CP ORF are shown in bold script.

either RNA 3/RNA 4 or xrRNAs involving 'coremin' might mediate template switching from RNA 3/RNA 4 to RNA 2 during minus-strand synthesis of virus replication, ultimately, resulting in chRNA formation. We tested this hypothesis by combining computational predictions, manual inspection of the sequences and mutagenesis. Indeed, manual inspection and the RNAfold algorithm predicted base-pairing interactions between 3′-proximal part of the CP ORF (nt 700–723) and 'coremin'. Additionally, a long SL structure immediately 3′-adjacent to the CP ORF was predicted as well. Fig. 3a shows an RNAfold-

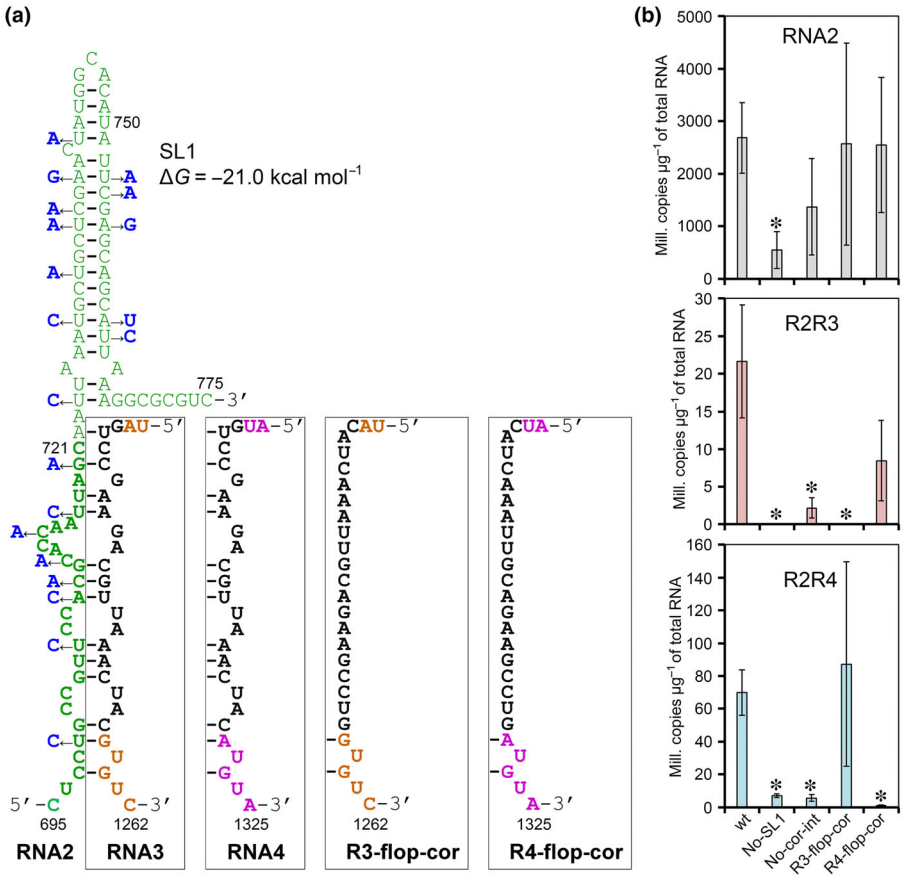

Fig. 4 Effect of SL1 mutations and mutations disrupting a putative base-pairing interaction between coremin and RNA2 on the accumulation chimeric RNAs in *Nicotiana benthamiana*. (a) Predicted stem-loop structure (SL1) in the beet soilborne mosaic virus (BSBMV) RNA2, and predicted base-pairing interaction between RNA 2 and RNA3/RNA4 involving 'coremin' (boxed). Numbering refers to nucleotide positions in the plus strand of full-length RNA2, RNA3 or RNA4, respectively. Silent mutations introduced to test SL1 and intermolecular base-pairing interaction requirements for chimeric RNA production are shown in blue script. Coramin sequence is shown in black script. RNA2 sequence that is incorporated into chimeric RNAs is shown in bold green script, whereas RNA3 and RNA4 sequences incorporated into chimeric RNAs are shown in brown and in magenta, respectively. The free energy refers to SL1. (b) Quantification of the accumulation of BSBMV RNA2 and chimeric RNAs by absolute RT-qPCR in the systemically infected leaves of *N. benthamiana* 21 dpi. Data are means ± SD; $n = 3$. Type of the mutant RNA replacing the corresponding RNA in the inoculum (RNA1 + RNA2 + RNA3 + RNA4, wt) is indicated below the graph. Asterisks indicate that the RNA accumulation values were significantly different compared with wt ($P < 0.05$, Student's two-tailed *t*-test). dpi, days postinoculation.

predicted stem-loop SL1 comprising two arms, nt 724–743 and nt 747–766, respectively.

Moreover, a structure similar to SL1 and the base-pairing interactions with 'coremin' were predicted when the RNAfold algorithm was applied to the plus strand of the genomic RNAs of BNYVV (RNA 2, RNA 3 and RNA 5, respectively) and two other benyviruses, burdock mottle virus (BuMV) and rice stripe necrosis virus (RSMV), suggesting conservation of these features in the genus *Benyvirus* (Fig. 3). Compared with 'coremin'-bearing BSBMV RNA 3 and RNA 4, BNYVV genomic components harbouring 'coremin' are represented by RNA 3 and RNA 5 (Fig. 3a).

To address the direct role of SL1 in chRNA production and validate our predictions, we introduced 12 silent point mutations into nt 724 to nt 768 of the CP-RTD ORF (Fig. 4a), and the obtained mutant was named No-SL1. To assess stability of the introduced mutations upon virus inoculation, 28 dpi total RNA was extracted from upper leaves, reverse transcribed, PCR amplified and sequenced. Interestingly, in most of the plants (13 out 17), No-SL1 mutant reverted back to wt (Table S2). However, stability of the introduced mutations was confirmed for 4 out of the 17 inoculated pants (Table S2). RT-qPCR analysis performed on total RNA preparations recovered from the samples of leaves systemically infected with No-SL1 with confirmed stable mutations revealed significant reduction in chRNA accumulation (Fig. 4b), although the accumulation of the genomic RNA 2 was also reduced *c.* 5.2-fold as compared to wt it accumulated at the readily detectable levels (Fig. 4b, upper panel). Thus, we concluded that point mutations disrupting SL1 inhibit chRNA production. The data are in agreement with our computational prediction of SL1 in the plus strand.

To specifically address the role of base-pairing between 'coremin' and RNA2 in chRNA production, three mutants, No-cor-int, R3-flop-cor and R4-flop-cor, were derived from RNA 2, RNA 3 and RNA 4 cDNA, respectively, by mutagenesis. Eight silent point mutations were engineered into 3′-proximal part of

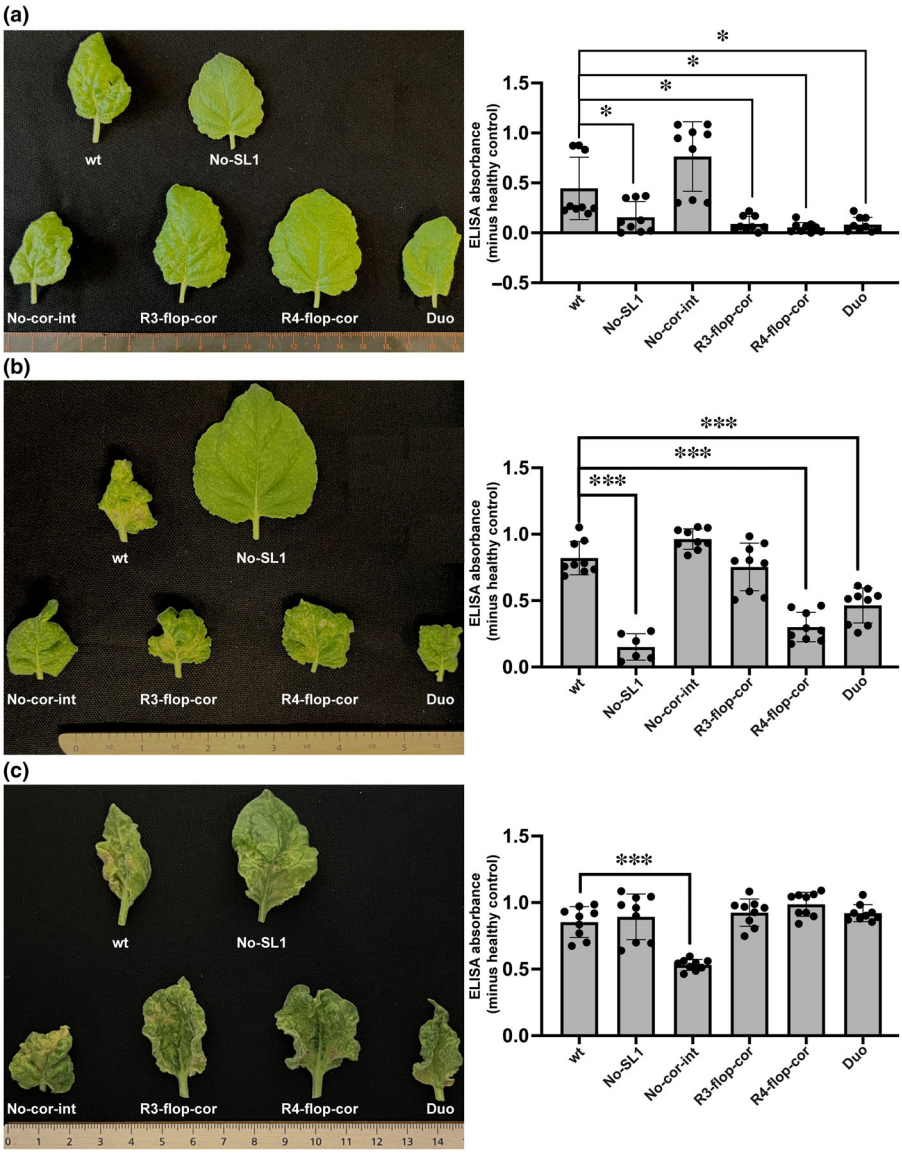

Fig. 5 Effect of SL1 mutations and mutations disrupting a putative base-pairing interaction between coremin and RNA2 and on virus pathogenicity as assayed at three time points, 9, 13 and 23 dpi, respectively in *Nicotiana benthamiana* plants. (a–c) Foliar symptoms on *N. benthamiana* produced by wt beet soilborne mosaic virus (BSBMV) and BSBMV mutants (left panels). Type of the mutant RNA replacing the corresponding RNA in the inoculum (RNA1 + RNA2 + RNA3 + RNA4, wt) is indicated below the image of the leaf and below the graph. Duo, RNA1 + RNA2 + R2R3 + R2R4. Detection of BSBMV CP antigen by enzyme-linked immunosorbent assay (ELISA) as indicated by absorbance values at 405 nm (right panels). Plant extracts were prepared from fifth (9 dpi), sixth (13 dpi) and seventh (23 dpi) leaf above inoculated, respectively, as shown in the left panel. Type of the inoculum is indicated below the graph. Data are means ± SD ($n = 9$). Asterisks indicate that the RNA accumulation values were significantly different compared with wt (*, $P < 0.05$; ***, $P < 0.01$, Student's two-tailed t-test). dpi, days postinoculation.

the CP ORF (nt 697–722) to create the mutant No-cor-int, in which the potential interaction of 3′-end of the CP cistron of RNA 2 with 'coremin' was disrupted (Fig. 4a). In R3-flop-cor and R4-flop-cor mutants, the sequence of 'coremin' was replaced by its reverse sequence (Fig. 4a). Subsequently, these mutants were inoculated on *N. benthamiana* leaves. All three inocula gave rise to viruses that were fully competent in long-distance movement, and viral RNAs were detected in upper noninoculated leaves (Fig. 4b). As before, stability of the mutations was confirmed by sequencing (Table S2), and only samples with stable mutations were taken for further analysis. RT-qPCR analysis performed on RNA isolated from the leaves of the plants systemically infected with No-cor-int, R3-flop-cor or R4-flop-cor revealed significant reduction in chRNA accumulation compared with the plants infected with wt virus (Fig. 4b). These results, therefore, indicate that potential partner sequences involving 'coremin' and 3′-end of the CP cistron of RNA 2 are required for the production of chRNAs.

To assess the effect of the chimeric RNAs on virus pathogenicity, the inocula containing the mutants were assembled as described above and inoculated on *N. benthamiana* leaves. An additional inoculum was assembled comprising RNA 1 + RNA 2 + R3-flop-cor + R4-flop-cor (named Duo). Development of BSBMV symptoms on upper noninoculated leaves was monitored at 8, 9, 13 and 23 dpi, whereas accumulation of BSBMV CP antigen was examined at 9, 13 and 23 dpi. First typical BSBMV symptoms were observed in upper *N. benthamiana* leaves as early as 8 dpi in all plants (two experiments, 12 plants in total) inoculated with wt virus, whereas all plants inoculated with the mutants remained symptomless (Fig. S7).

Nine days postinoculation some mild symptoms could be observed on upper leaves of the plants inoculated with the mutants, whereas plants inoculated with wt virus developed severe symptoms (Fig. 5a). The ELISAs performed on extracts prepared from the fifth leaf above inoculated 9 dpi clearly showed the differences in accumulation of the CP antigen (Fig. 5a, right

panel), as four mutants accumulated significantly less CP antigen ($P < 0.05$) compared with wt and No-cor-int mutant, which rapidly reverted back to wt (Table S2). Moreover, similar trend was also observed at 13 dpi when ELISAs were performed on extracts prepared from six leaves above the inoculated (Fig. 5b, right panel). At this time point, plants infected with the mutants showed the symptoms similar to wt (Fig. 5b, left panel), with the exception of plants infected with No-SL1 mutant, which remained symptomless (Fig. 5b, left panel). The levels of CP accumulation were significantly lower in plants infected with No-SL1, R4-flop-cor and R3-flop-cor + R4-flop-cor (Duo) mutants as compared to wt (Fig. 5b, right panel), whereas CP accumulated at the levels similar to wt in plants infected with No-cor-int and R3-flop-cor mutants (Fig. 5b, right panel), which reverted back to wt by 13 dpi.

Twenty-three days postinoculation, the symptoms in all infected plants and the levels of CP accumulation were undistinguishable from wt (Fig. 5c). Notably, the levels of CP accumulation were significantly lower in plants infected with No-SL1 mutant than those in wt owing to severe necrotisation of leaf tissue (Fig. 5c). Overall, our results show that BSBMV infection is delayed, less symptoms are induced and less CP accumulates if mutations disrupt formation of chimeric RNAs.

NbXRN4 knockdown inhibits biogenesis of both xrRNAs and chimeric RNAs

Having determined that a base-pairing between 'coremin' and RNA 2 is needed for chRNA production, we next wanted to resolve whether interaction of RNA 2 with 'coremin' of genomic RNAs (i.e. RNA 3 and RNA 4) or with 'coremin' of noncoding xrRNAs is required for chRNA production. To this end, we used virus-induced gene silencing (VIGS) to knockdown the expression of *NbXRN4*, a gene encoding Xrn4 5′–3′ exoribonuclease essential for production of noncoding xrRNAs of BNYVV (Flobinus *et al.*, 2018). Considering that both BNYVV and BSBMV have identical 'coremin' sequence we assumed that, similar to BNYVV, in BSBMV 'coremin' and its adjacent sequence (Dilweg *et al.*, 2019) could stall Xrn4 (Flobinus *et al.*, 2018) leading to xrRNA production. We validated the down-regulation of *NbXRN4* by RT-qPCR 14 dpi (Fig. 6a). Moreover, knockdown of *NbXRN4* expression led to a severe developmental phenotype characterised by overall stunting of the *NbXRN4*-silenced plants (Fig. 6b). *NbXRN4*-silenced and control plants were inoculated with BSBMV and the accumulation of genomic RNA 2, RNA 3 and RNA 4, as well as the noncoding xrRNAs and chRNAs was monitored by RT-qPCR in systemically infected upper leaves 21 dpi.

We used quantification of the plus- and minus strand of xrRNAs as a read-out for xrRNA accumulation. To this end, we developed a quantitative stem-loop RT-qPCR (Fig. S8), the method initially developed for quantification of miRNAs and siRNAs (Varkonyi-Gasic & Hellens, 2011; Kalyandurg *et al.*, 2019). RT-qPCR data showed the accumulation of both xrRNAs (both of plus and minus strands) and chRNAs in upper leaves of the plants silenced for *NbXRN4* was decreased markedly as compared to control plants (Fig. 6c–e), whereas the accumulation of the viral genomic RNAs dramatically increased (up to 2.9-fold for RNA 2, up to 11.3-fold for RNA 3 and up to 1.9-fold for RNA 4; Fig. 6c). Interestingly, the increase in CP accumulation in the *NbXRN4* knockdown plants was not as dramatic as an increase in viral RNA levels, probably due to a significant decrease in CP-encoding chimeric RNAs (Fig. 6f). Hence, collectively, the results show that knockdown *NbXRN4* expression led to inhibition of chRNA production. Moreover, decrease in the chRNA production correlated with lower levels of xrRNAs accumulation.

Discussion

General features of chimeric RNAs

We present several observations documenting new aspects of the functioning of viral RNA genomes. In this paper, novel naturally occurring viral RNA species derived from BSBMV RNA 2 and RNA 3/RNA 4 were discovered and characterised and the potential mechanism of their biogenesis was addressed. The evidence suggests that the novel RNA species, the chRNAs, are most likely the products of template switching on a putative intermolecular base-pairing complex between RNA 2 and xrRNAs, RNA structure-dependent exoribonuclease-resistant noncoding derivatives of RNA 3 and RNA 4. These findings establish chRNAs as a distinct functional class of viral RNAs and suggest that 'coremin' of xrRNAs can be involved in intermolecular base-pairing interactions, which, followed by replication, can lead to production of chRNA species.

To the best of our knowledge, this is the first report of naturally occurring functional (CP-encoding and moving systemically) chRNA; however, chRNAs consisting of partial sequences of RNA 3 and RNA 4 were previously detected after serial mechanical passages of BNYVV, a virus related to BSBMV (D'Alonzo *et al.*, 2012). Hence, by contrast to our study, it is currently unclear whether RNA 3/RNA 4 derived chRNAs exist within the natural population of BNYVV or just represent another class of aberrant RNA molecules generated by serial mechanical passages of a virus in the laboratory. Two forms of viral D-RNAs designated as a D-RNA-A (2082 nt) and a D-RNA-B (1802 nt) associated with the potato yellow vein virus (PYVV; genus *Crinivirus*, family Closteroviridae) infections (Eliasco *et al.*, 2006). Both D-RNAs are A/U-rich and characterised by the presence of the 5′-termini originating from the 5′-end of RNA 1 (85% identity) and the 3′-termini coming from the 3′-UTR of RNA 3 (92% identity) and were suggested to represent erroneous products of genetic recombination (Eliasco *et al.*, 2006). Formally, capped mRNA molecules produced during transcription of viruses with negative-sense RNA genomes can be considered chRNA as well because viruses of Orthomyxoviridae (infecting humans and animals) and of the order of Bunyavirales including family Tospoviridae (infecting plants) acquire the 5′-end from capped cellular mRNAs through cap-snatching mechanism, which involves endonucleolytic cleavage of cellular mRNAs several bases downstream of the cap structure to generate genetic hybrids of host and virus mRNAs (De Vlugt *et al.*, 2018; Olschewski *et al.*, 2020).

Mechanism of chRNA biogenesis

The detailed mechanism by which chRNAs are produced during virus replication cycles remains to be discovered. However, several observations emphasise the role of xrRNAs in chRNA biogenesis. In general, xrRNAs are able to block various exoribonucleases and, therefore, act as mechanical blocks to such enzymes (MacFadden *et al.*, 2018; Steckelberg *et al.*, 2018a,b). In plants, Xrn4 is a major cytoplasmic 5′→3′ exoribonuclease

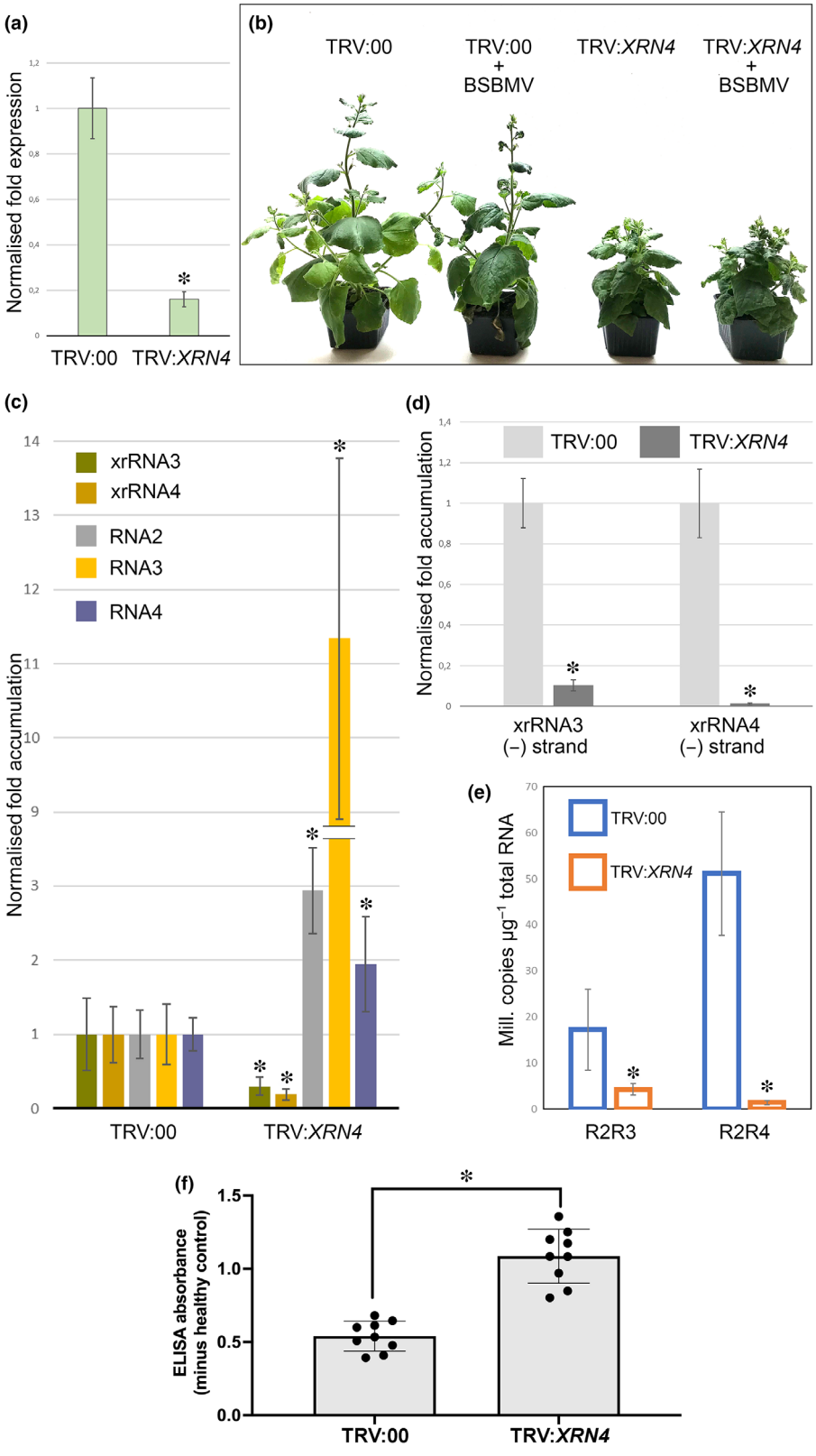

Fig. 6 *NbXRN4* knockdown inhibits biogenesis of both exoribonuclease-resistant RNAs (xrRNAs) and chimeric RNAs in *Nicotiana benthamiana*. (a) Gene silencing of *NbXRN4* in TRV:*XRN4*-infected plants. Total RNAs were extracted from the upper leaves 14 dpi and were used for RT-qPCR. Data are means ± SD ($n = 16$). *NbF-BOX* and *NbPP2A* were used as normalisation controls. (b) Phenotypes of the plants silenced for *NbXRN4*. (c) Relative fold accumulation of beet soilborne mosaic virus (BSBMV) xrRNAs and genomic RNAs in plants silenced for *NbXRN4* and normalised to the expression of *NbPP2A*. Data are means ± SD ($n = 6$). Asterisks indicate significant statistical difference relative to TRV:00 control; *, $P < 0.05$; Student's two-tailed *t*-test. xrRNA3 and xrRNA4 were quantified by a stem-loop (SL) RT-qPCR. (d) Relative fold accumulation of minus strand of xrRNA3 and xrRNA4 as quantified by SL RT-qPCR. *NbPP2A* was used as normalisation control. Data are means ± SD ($n = 3$). Asterisks indicate significant statistical difference relative to TRV:00 control; *, $P < 0.05$; Student's two-tailed *t*-test. (e) Quantification of the accumulation of BSBMV chimeric RNAs by absolute RT-qPCR in the upper leaves of *N. benthamiana* plants infected with TRV:00 (control) or TRV:*XRN4* (*XRN4* knockdown) 21 dpi. Data are means ± SD ($n = 3$). Asterisks indicate significant statistical difference relative to TRV:00 control; *, $P < 0.05$; Student's two-tailed *t*-test. (f) Detection of BSBMV CP antigen by enzyme-linked immunosorbent assay (ELISA) as indicated by absorbance values at 405 nm. Plant extracts were prepared from upper systemically infected leaves at 21 dpi. Type of the inoculated plants is indicated below the graph. Data are means ± SD ($n = 9$). *, $P < 0.0001$; Student's two-tailed *t*-test. dpi, days postinoculation.

belonging to the large family of eukaryotic XRN proteins (Nagarajan *et al.*, 2013). In this study, knockdown of *XRN4* expression resulted in inhibition of production of both xrRNAs and chRNAs, thus emphasising the significance of Xrn4 activity (and subsequently, xrRNAs) for chRNA biogenesis.

Collectively, the data suggest that all three features, namely, intermolecular base-pairing interactions, a stem-loop structure (SL1) in RNA 2 and Xrn-resistant noncoding RNAs (xrRNAs), investigated in this study are essential for chRNA formation and disruption of any of these features results in inhibition of chRNA biogenesis. Additionally, the results pointed out to significance of SL1 integrity for the virus infection cycle as the mutants, harbouring silent mutations that disrupt SL1, reverted back to wt in most of the cases and the nonreverted mutants accumulated at significantly lower levels compared to wt.

Interestingly, a putative intermolecular base-pairing interaction complex between RNA 2 and xrRNAs and the stem-loop structure (SL1) are located in extremely close proximity to each other and, literally, separated by a single nucleotide residue. While we have no direct assay to measure or visualise formation of these structures yet and can thus not rule out other or additional mechanisms, our mutagenesis data reveal absolute requirement of these putative aforementioned features for the chRNA biogenesis. Computational predictions supported by mutagenesis invite speculation that these unique topology (Figs 3, 7) acts as mechanical block to hinder viral RNA-dependent RNA polymerase during synthesis of the minus strand on the xrRNA template that base-pairs with RNA 2, and to facilitate subsequent template switching from xrRNA to RNA2 (Fig. 7). We suspect that the RNA polymerase can unwind base-pairing interaction of xrRNA with RNA 2 mediated by 'coremin', but, immediately after that, SL1 stalls the RNA polymerase (Fig. 7). We further speculate that RNA polymerase stalling does not result in release of the newly synthesised minus strand, instead, the RNA polymerase continues synthesis on the RNA 2 template (Fig. 7). In general, viral RNA polymerases have high affinity to highly structured (harbouring SL structures) 3′- and 5′-temini of viral genomic RNAs (Kawamura-Nagaya *et al.*, 2014; Ishibashi & Ishikawa, 2016); thus, it is possible that the RNA polymerase binds to a 19-nt-long SL1 resulting in the RNA polymerase stalling and template switching (Fig. 7). This model could explain the requirements of SL1, base-pairing interaction between RNA 2 and 'coremin' for chRNA biogenesis (Fig. 7). Ultimately, synthesis of the plus strand on the chimeric minus strand

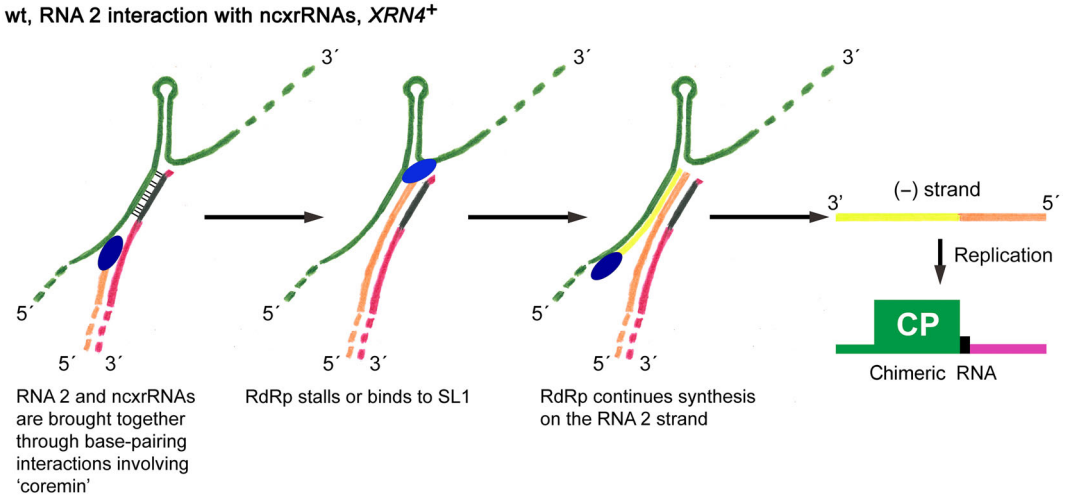

Fig. 7 A model for chimeric RNA biogenesis. RNA 2 is indicated in green, noncoding exoribonuclease-resistant RNAs (xrRNA) is shown in magenta, 'coremin' is indicated in black. Slanted black lines indicate complementarity between RNA 2 and 'coremin'. Viral RNA-dependent RNA polymerase is represented by a dark blue ellipsoid. SL1, stem-loom structure. ncxrRNA, noncoding exoribonuclease-resistant RNA.

generates a biologically active smaller CP-encoding chRNAs capable of long-distance movement and active translation to yield viral CP for encapsidation. Potentially, base-pairing interaction mediated by 'coremin' can be formed between full-length RNA 2 and RNA 3/RNA 4, but we suspect that the template switching from RNA 3/RNA 4 to RNA 2 does not occur in here because RNA polymerase does not need to dissociate from the RNA 3/RNA 4 template after unwinding the base-pairing interaction of RNA 3/RNA 4 with RNA 2 mediated by 'coremin' and just continues the synthesis (Fig. S9). This speculation is supported by the lack of chRNA formation (and accumulation of xrRNAs) in the *XRN4* knockdown plants infected with BSBMV, in which only full-length BSBMV genomic RNAs, but not xrRNAs, can be readily detected.

The mechanism of chRNA production suggested in this study somewhat resembles discontinuous RNA synthesis in the order Nidovirales including coronaviruses (van Vliet *et al.*, 2002; Sola *et al.*, 2015; Kim *et al.*, 2020). This process of sgRNA synthesis is unique to the order Nidovirales and is characterised by the presence of the common 'leader' sequence of 65–95 nt residues in different coronaviruses fused to the downstream 'body' sequence 3′-coterminal with virus genome (Kim *et al.*, 2020). The prevailing model implies that leader-to-body fusion occurs during synthesis of the negative-strand RNA at short motifs called transcription-regulatory sequences (TRSs) that precede each viral gene. Each TRS contains a conserved 6–7 nt core sequence (CS) surrounded by variable sequences. During negative-strand synthesis, viral RNA polymerase pauses when it crosses a TRS in the body (TRS-B) and switches the template to the TRS in the leader (TRS-L) through base-pairing between the CS of the leader and the complementary CS of the body. This results in discontinuous transcription leading to a set leader-body fused negative-strand sgRNAs, which subsequently serve as templates for the synthesis of numerous copies of sgRNA. This discontinuous transcription mechanism bear a resemblance to high-frequency, similarity-assisted copy-choice RNA recombination that requires sequence identity between donor and acceptor RNAs and hairpin structures present in the acceptor RNA (Nagy & Simon, 1997). Hence, the TRS-L forming hairpin would act as an acceptor for the complimentary TRS-B donor sequence. The sequences and secondary structures of the RNA motifs involved in these long-distance interactions are conserved among coronaviruses suggesting a functional similarity during sgRNA synthesis (Kim *et al.*, 2020). Similarly, in this study, chRNAs are synthesised by fusion of noncontiguous sequences, the 5′-end of RNA 2 (including complete CP ORF) and 3′-UTR of either RNA 3 or RNA 4. Moreover, base-pairing interaction of 'coremin' with the 3′-proximal part of the CP cistron resembles the base-pairing between the CS of the leader and the complementary CS of the body (see above), whereas SL1 serves as a facilitator of the template switching.

Role of chRNAs in virus pathogenesis

Notably, both chimeric RNAs reported in this study possess a full-length ORF encoding CP. Translation of these chimeric RNAs would yield extra copies of CP. Indeed, our experiments using recombinant viruses show that CP can be translated from the chimeric RNA and is readily detectable by ELISA (Fig. 2e). These findings provide further evidence that the chimeric RNAs are translationally functional besides moving systemically. Adoption by benyviruses of an alternative mechanism for CP synthesis through the formation of monocistronic (vs polycistronic CP-encoding genomic RNA 2) might therefore alter viral replication kinetics and virus yield. Indeed, the time-course experiments show that mutations disrupting the formation of chimeric RNA lead to a delay in the establishment of the virus infection manifested as a delay in the onset of the BSBMV-specific symptoms in the systemically infected plants and lower accumulation of the CP antigen (Fig. 5). An appealing hypothesis is that the short chimeric monocistronic RNA is translated more efficiently than the long polycistronic genomic RNA 2. Several mechanisms might contribute to that. Most eukaryotic mRNAs are translated via cap- and scanning-dependent initiation mechanism (Sonenberg & Hinnebusch, 2009; Aitken & Lorsch, 2012). The main scaffolding subunit eIF4G of the 5′ cap-bound eIF4F complex (cap-binding complex) recruits the ribosome by binding eIF3 and circularises the mRNA by binding poly(A)-binding proteins (Gingras *et al.*, 1999; Borden, 2016). Recent evidence indicates that eukaryotic mRNAs are circularised, potentially permitting terminating ribosomes to preferentially reinitiate on the same RNA molecule (Rogers *et al.*, 2017). By bringing the sites of translational initiation and termination into close proximity through circularisation of the mRNA, the closed-loop complex allows ribosomes that have just finished translation to reinitiate on the same mRNA template instead of returning to the cytoplasmic pool. BSBMV genomic and sgRNAs have 5′ cap and poly(A)-tail at the 3′ ends suggesting that these features are also present at the ends of chimeric RNAs. Circularisation of monocistronic chimeric RNAs might make recycling of the ribosomes on the same template easier compared with long polycistronic RNAs, thus promoting translation on chimeric RNAs, which would yield more CP.

Absolute quantification of BSBMV RNAs revealed that chimeric RNAs are much more abundant compared to genomic RNA2 (Figs 1c, S2) suggesting that besides being replicated (as short molecules) more efficiently chimeric RNAs might escape or might be not susceptible to a host defence mechanism targeting virus genomic RNAs. The most obvious candidate for this role is nonsense-mediated decay NMD. NMD is a host RNA quality control pathway that recognises and destroys RNAs with internal termination codons and long 3′-UTRs (Kervestin & Jacobson, 2012). NMD also serves as a general viral restriction mechanism against positive-sense RNA viruses because genomes of many viruses are organised into polycistronic mRNA with only 5′-proximal ORF being directly translated whereas the rest of the sequence is expressed via production sgRNAs and, thus, can be perceived by NMD machinery as a long 3′-UTR with stop codons (Garcia *et al.*, 2014; May *et al.*, 2020). Viruses susceptible to NMD targeting evolved various strategies to evade NMD that include *cis*-acting RNA elements and *trans*-acting viral proteins (May *et al.*, 2018, 2020). We speculate that generation of chimeric RNAs might be another strategy to circumvent NMD targeting of CP-encoding BSBMV RNA2 on the early stages of

virus infection, thus boosting CP production and facilitating infection.

Conservation of 'coremin' sequence

Notably, both BNYVV and BSBMV share identical 'coremin' sequences (Flobinus *et al.*, 2016). Moreover, when applied to BNYVV and two newly reported benyviruses BuMV and RSMV (Kondo *et al.*, 2013; Bagayoko *et al.*, 2021), RNAfold algorithms predict and overall topology (intermolecular base-pairing interactions + adjacent SL1) similar to that of BSBMV (Fig. 3), suggesting conservation of these folds at least in the genus *Benyvirus*. Although, so far, RSMV and BuMV are reported to have bipartite genome and do not have 'coremin'-harbouring RNAs, interactions between 'coremin' and 3′-proximal part of the CP cistron can be predicted as well (Fig. 3).

Concluding remarks and further perspectives

Although chRNAs have not yet been found in other viruses (with the exception of D-RNA-A and D-RNA-B of PYVV, see above), this might be due to the limitation of the computational algorithms used nowadays for mining for viral sequences in RNA-Seq data as the viral sequences are mostly mapped to the virus reference genome. *De novo* assembly of the viral reads or more recently introduced the nanopore-based direct RNA sequencing (DRS) approach might resolve these issues and, potentially, lead to discovery of chRNAs associated with other viruses. When applied to characterisation of the coronavirus transcriptome, DRS approach resulted in identification of numerous unconventional RNA joining events (additional unconventional sgRNAs) in addition to 10 canonical sgRNAs (Kim *et al.*, 2020). To our knowledge, there are no other examples of intermolecular base-pairing complex formation leading to the production of functional chRNAs, but our discovery suggests that similar mechanisms may operate elsewhere.

Thus, this study implies that benyviruses usurp Xrn4 robust degradation activity as a part of elegant RNA maturation pathway to generate monocistronic CP-encoding chRNAs through intermolecular RNA–RNA interactions. Involvement of xrRNAs in the intermolecular RNA–RNA interactions may be a more common mechanism than anticipated so far, and recent studies have identified putative xrRNAs and 'coremin'-like sequences in several virus families, including Betaflexiviridae, Tombusviridae, Secoviridae, Potyviridae and Virgaviridae (Steckelberg *et al.*, 2018a,b; Dilweg *et al.*, 2019). Overall, our discoveries suggest that the roles of xrRNAs in virus infection cycle might be more diverse than previously appreciated.

Acknowledgements

This work was funded by The Swedish Foundation for Strategic Research (SSF; grant SM14-0032 to EIS) and The Swedish Research Council for Sustainable Development FORMAS (grants 2018-00591 and 2021-00898 to EIS).

Competing interests

None declared.

Author contributions

B-LL, EIS and MV planned and designed the research. B-LL, EIS, EP, JFG, KN, MM and SL performed experiments, conducted fieldwork and analysed data. EIS, KN, MM, MV and SL reviewed the manuscript. EIS wrote the paper.

ORCID

Jose F. Gil https://orcid.org/0000-0003-2749-2490
Sebastian Liebe https://orcid.org/0000-0002-4728-9548
Eugene I. Savenkov https://orcid.org/0000-0002-5802-5089
Mark Varrelmann https://orcid.org/0000-0003-1014-5185

Data availability

All chimeric RNA sequences have been deposited in the NCBI database: the chimeric RNA R2R3 (accession no. AX469403), the chimeric RNA R2R4 (accession no. AX469404) and the chimeric RNA encompassing the 5′-terminal 724 nt of BSBMV RNA 2 and 3′-terminal 545 nts of BNYVV (accession number AX469405). All data needed to evaluate the conclusions of the paper are present in the paper and in the Supporting Information. Plasmids and reagents can be provided by MV and EIS pending scientific review and a completed material transfer agreement. Request for these materials should be submitted to MV and EIS.

References

Aitken CE, Lorsch JR. 2012. A mechanistic overview of translation initiation in eukaryotes. *Nature Structural & Molecular Biology* **19**: 568–576.

Akiyama BM, Laurence HM, Massey AR, Costantino DA, Xie X, Yang Y, Shi PY, Nix JC, Beckham JD, Kieft JS. 2016. Zika virus produces noncoding RNAs using a multi-pseudoknot structure that confounds a cellular exonuclease. *Science* **354**: 1148–1152.

Bagayoko I, Celli MG, Romay G, Poulicard N, Pinel-Galzi A, Julian C, Filloux D, Roumagnac P, Sérémé D, Bragard C *et al.* 2021. Genetic diversity of rice stripe necrosis virus and new insights into evolution of the genus *Benyvirus*. *Viruses* **13**: 737.

Bertran A, Ciuffo M, Margaria P, Rosa C, Resende RO, Turina M. 2016. Host-specific accumulation and temperature effects on the generation of dimeric viral RNA species derived from the S-RNA of members of the *Tospovirus* genus. *Journal of General Virology* **97**: 3051–3062.

Bidet K, Dadlani D, Garcia-Blanco MA. 2014. G3BP1, G3BP2 and CAPRIN1 are required for translation of interferon stimulated mRNAs and are targeted by a dengue virus non-coding RNA. *PLoS Pathogens* **10**: e1004242.

Blum C, Gotsch S, Heinze C. 2017. Duplications in the 3′ termini of three segments of *Fusarium graminearum* virus China 9. *Archives of Virology* **162**: 897–900.

Borden KL. 2016. The eukaryotic translation initiation factor eIF4E wears a "cap" for many occasions. *Translation* **4**: e1220899.

Charley PA, Wilusz CJ, Wilusz J. 2018. Identification of phlebovirus and arenavirus RNA sequences that stall and repress the exoribonuclease XRN1. *Journal of Biological Chemistry* **293**: 285–295.

Chiba S, Hleibieh K, Delbianco A, Klein E, Ratti C, Ziegler-Graf V, Bouzoubaa S, Gilmer D. 2013. The benyvirus RNA silencing suppressor is essential for

long-distance movement, requires both zinc-finger and NoLS basic residues but not a nucleolar localization for its silencing-suppression activity. *Molecular Plant–Microbe Interactions* **26**: 168–181.

D'Alonzo M, Delbianco A, Lanzoni C, Autonell CR, Gilmer D, Ratti C. 2012. Beet soil-borne mosaic virus RNA-4 encodes a 32 kDa protein involved in symptom expression and in virus transmission through *Polymyxa betae*. *Virology* **423**: 187–194.

De Vlugt C, Sikora D, Pelchat M. 2018. Insight into influenza: a virus cap-snatching. *Viruses* **10**: 641.

Dilweg IW, Gultyaev AP, Olsthoorn RC. 2019. Structural features of an Xrn1-resistant plant virus RNA. *RNA Biology* **16**: 838–845.

Eliasco E, Livieratos IC, Müller G, Guzman M, Salazar LF, Coutts RHA. 2006. Sequences of defective RNAs associated with potato yellow vein virus. *Archives of Virology* **151**: 201–204.

Flobinus A, Chevigny N, Charley PA, Seissler T, Klein E, Bleykasten-Grosshans C, Ratti C, Bouzoubaa S, Wilusz J, Gilmer D. 2018. Beet necrotic yellow vein virus noncoding RNA production depends on a 5′→3′ Xrn exoribonuclease activity. *Viruses* **10**: 137.

Flobinus A, Hleibieh K, Klein E, Ratti C, Bouzoubaa S, Gilmer D. 2016. A viral noncoding RNA complements a weakened viral RNA silencing suppressor and promotes efficient systemic host infection. *Viruses* **8**: 272.

Ganser LR, Kelly ML, Herschlag D, Al-Hashimi HM. 2019. The roles of structural dynamics in the cellular functions of RNAs. *Nature Reviews Molecular Cell Biology* **20**: 474–489.

Garcia D, Garcia S, Voinnet O. 2014. Nonsense-mediated decay serves as a general viral restriction mechanism in plants. *Cell Host & Microbe* **16**: 391–402.

Gibson DG, Young L, Chuang R-Y, Venter JC, Hutchison CA 3rd, Smith HO. 2009. Enzymatic assembly of DNA molecules up to several hundred kilobases. *Nature Methods* **6**: 343–345.

Gil JF, Liebe S, Thiel H, Lennefors B-L, Kraft T, Gilmer D, Maiss E, Varrelmann M, Savenkov EI. 2018. Massive up-regulation of LBD transcription factors and EXPANSINs highlights the regulatory programs of rhizomania disease. *Molecular Plant Pathology* **19**: 2333–2348.

Gil JF, Wibberg D, Eini O, Savenkov EI, Varrelmann M, Liebe S. 2020. Comparative transcriptome analysis provides moleculari into the interaction of beet necrotic yellow vein virus and beet soil-borne mosaic virus with their host sugar beet. *Viruses* **12**: 76.

Gilmer D, Bouzoubaa S, Hehn A, Guilley H, Richards K, Jonard G. 1992. Effcient cell-to-cell movement of beet necrotic yellow vein virus requires 3′ proximal genes located on RNA 2. *Virology* **189**: 40–47.

Gilmer D, Ratti C, Michel F. 2018. Long-distance movement of helical multipartite phytoviruses: keep connected or die? *Current Opinion in Virology* **33**: 120–128.

Gingras AC, Raught B, Sonenberg N. 1999. eIF4 initiation factors: effectors of mRNA recruitment to ribosomes and regulators of translation. *Annual Review of Biochemistry* **68**: 913–963.

Ishibashi K, Ishikawa M. 2016. Replication of tobamovirus RNA. *Annual Review of Phytopathology* **54**: 55–78.

Janssen S, Giegerich R. 2015. The RNA shapes studio. *Bioinformatics* **31**: 423–425.

Johnson PZ, Kasprzak WK, Shapiro BA, Simon AE. 2019. RNA2Drawer: geometrically strict drawing of nucleic acid structures with graphical structure editing and highlighting of complementary subsequences. *RNA Biology* **16**: 1667–1671.

Kalyandurg PB, Tahmasebi A, Vetukuri RR, Kushwaha SK, Lezzhov AA, Solovyev AG, Grenville-Briggs LJ, Savenkov EI. 2019. Efficient RNA silencing suppression activity of potato mop-top virus 8K protein is driven by variability and positive selection. *Virology* **535**: 111–121.

Kawamura-Nagaya K, Ishibashi K, Huang Y-P, Miyashita S, Ishikawa M. 2014. Replication protein of tobacco mosaic virus cotranslationally binds the 5′ untranslated region of genomic RNA to enable viral replication. *PNAS* **111**: 1620–1628.

Kervestin S, Jacobson A. 2012. NMD: a multifaceted response to premature translational termination. *Nature Reviews Molecular Cell Biology* **13**: 700–712.

Kim D, Lee J-Y, Yang J-S, Kim JW, Kim VN, Chang H. 2020. The architecture of SARS-CoV-2 transcriptome. *Cell* **181**: 914–921.

Koenig R, Haeberle A, Commandeur U. 1997. Detection and characterization of a distinct type of beet necrotic yellow vein virus RNA 5 in a sugarbeet growing area in Europe. *Archives of Virology* **142**: 1499–1504.

Kondo H, Hirano S, Chiba S, Andika IB, Hirai M, Maeda T, Tamada T. 2013. Characterization of burdock mottle virus, a novel member of the genus benyvirus, and the identification of benyvirus-related sequences in the plant and insect genomes. *Virus Research* **177**: 75–86.

Lauber E, Guilley H, Tamada T, Richards KE, Jonard G. 1998. Vascular movement of beet necrotic yellow vein virus in beta macrocarpa is probably dependent on an RNA 3 sequence domain rather than a gene product. *Journal of General Virology* **79**: 385–393.

Laufer M, Mohammad H, Maiss E, Richert-Pöggeler K, Dall'Ara M, Ratti C, Gilmer D, Liebe S, Varrelmann M. 2018. Biological properties of beet soil-borne mosaic virus and beet necrotic yellow vein virus cDNA clones produced by isothermal *in vitro* recombination: Insights for reassortant appearance. *Virology* **518**: 25–33.

Lee L, Telford EB, Batten JS, Scholthof KB, Rush CM. 2001. Complete nucleotide sequence and genome organization of beet soilborne mosaic virus, a proposed member of the genus *Benyvirus*. *Archives of Virology* **146**: 2443–2453.

Liu Y, Liu H, Zou J, Zhang B, Yuan Z. 2014. Dengue virus subgenomic RNA induces apoptosis through the Bcl-2-mediated PI3k/Akt signaling pathway. *Virology* **448**: 15–25.

Liu Y, Schiff M, Dinesh-Kumar SP. 2002. Virus-induced gene silencing in tomato. *The Plant Journal* **31**: 777–786.

Lukhovitskaya NI, Thaduri S, Garushyants SK, Torrance L, Savenkov EI. 2013. Deciphering the mechanism of defective interfering RNA (DI RNA) biogenesis reveals that a viral protein and the DI RNA act antagonistically in virus infection. *Journal of Virology* **87**: 6091–6103.

MacFadden A, O'Donoghue Z, Silva PAGC, Chapman EG, Olsthoorn RC, Sterken MG, Pijlman GP, Bredenbeek PJ, Kieft JS. 2018. Mechanism and structural diversity of exoribonuclease-resistant RNA structures in flaviviral RNAs. *Nature Communications* **9**: 119.

Manokaran G, Finol E, Wang C, Gunaratne J, Bahl J, Ong EZ, Tan HC, Sessions OM, Ward AM, Gubler DJ *et al.* 2015. Dengue subgenomic RNA binds TRIM25 to inhibit interferon expression for epidemiological fitness. *Science* **350**: 217–221.

May JP, Johnson PZ, Ilyas M, Gao F, Simon AE. 2020. The multifunctional long-distance movement protein of pea enation mosaic virus 2 protects viral and host transcripts from nonsense-mediated decay. *MBio* **11**: e00204-220.

May JP, Yuan X, Sawicki E, Simon AE. 2018. RNA virus evasion of nonsense-mediated decay. *PLoS Pathogens* **14**: e1007459.

Moon SL, Anderson JR, Kumagai Y, Wilusz CJ, Akira S, Khromykh AA, Wilusz J. 2012. A noncoding RNA produced by arthropod-borne flaviviruses inhibits the cellular exoribonuclease XRN1 and alters host mRNA stability. *RNA* **18**: 2029–2040.

Moon SL, Blackinton JG, Anderson JR, Dozier MK, Dodd BJT, Keene JD, Wilusz CJ, Bradrick SS, Wilusz J. 2015a. XRN1 stalling in the 5' UTR of Hepatitis C virus and bovine viral diarrhea virus is associated with dysregulated host mRNA stability. *PLoS Pathogens* **11**: e1004708.

Moon SL, Dodd BJT, Brackney DE, Wilusz CJ, Ebel GD, Wilusz J. 2015b. Flavivirus sfRNA suppresses antiviral RNA interference in cultured cells and mosquitoes and directly interacts with the RNAi machinery. *Virology* **485**: 322–329.

Nagarajan VK, Jones CI, Newbury SF, Green PJ. 2013. XRN 5′→3′ exoribonucleases: structure, mechanisms and functions. *Biochimica et Biophysica Acta* **1829**: 590–603.

Nagy PD, Simon AE. 1997. New insights into the mechanisms of RNA recombination. *Virology* **235**: 1–9.

Niehl A, Varrelmann M, Koenig R. 2021. Benyviruses (Benyviridae). In: Bamford DH, Zuckerman M, eds. *Encyclopedia of virology*. Amsterdam, the Netherlands: Elsevier, 603–611.

Olmos A, Bertolini E, Gil M, Cambra M. 2005. Real-time assay for quantitative detection of non-persistently transmitted plum pox virus RNA targets in single aphids. *Journal of Virological Methods* **128**: 151–155.

Olschewski S, Cusack S, Rosenthal M. 2020. The cap-snatching mechanism of bunyaviruses. *Trends in Microbiology* **28**: 293–303.

Onate-Sanchez L, Vicente-Carbajosa J. 2008. DNA-free RNA isolation protocols for *Arabidopsis thaliana*, including seeds and siliques. *BMC Research Notes* **1**: 93.

Pathak KB, Nagy PD. 2009. Defective interfering RNAs: foes of viruses and friends of virologists. *Viruses* **1**: 895–919.

Peltier C, Klein E, Hleibieh K, D'Alonzo M, Hammann P, Bouzoubaa S, Ratti C, Gilmer D. 2012. Beet necrotic yellow vein virus subgenomic RNA3 is a cleavage product leading to stable non-coding RNA required for long-distance movement. *Journal of General Virology* **93**: 1093–1102.

Pijlman GP, Funk A, Kondratieva N, Leung J, Torres S, van der Aa L, Liu WJ, Palmenberg AC, Shi P-Y, Hall RA *et al.* 2008. A highly structured, nuclease-resistant, noncoding RNA produced by flaviviruses is required for pathogenicity. *Cell Host & Microbe* **4**: 579–591.

Ratti C, Hleibieh K, Bianchi L, Schirmer A, Autonell CR, Gilmer D. 2009. Beet soil-borne mosaic virus RNA-3 is replicated and encapsidated in the presence of BNYVV RNA-1 and -2 and allows long distance movement in *Beta macrocarpa*. *Virology* **385**: 392–399.

Roby JA, Pijlman GP, Wilusz J, Khromykh AA. 2014. Noncoding subgenomic flavivirus RNA: multiple functions in West Nile virus pathogenesis and modulation of host responses. *Viruses* **6**: 404–427.

Rogers DW, Böttcher MA, Traulsen A, Greig D. 2017. Ribosome reinitiation can explain length-dependent translation of messenger RNA. *PLOS Computational Biology* **13**: e1005592.

Sambrook J, Fritsch EF, Maniatis T. 1989. *Molecular cloning: a laboratory manual, 2nd edn.* Cold Spring Harbor, NY, USA: Cold Spring Harbor Laboratory Press.

Sato K, Hamada M, Asai K, Mituyama T. 2009. CENTROIDFOLD: a web server for RNA secondary structure prediction. *Nucleic Acids Research* **37**: 277–280.

Schnettler E, Sterken MG, Leung JY, Metz SW, Geertsema C, Goldbach RW, Vlak JM, Kohl A, Khromykh AA, Pijlman GP. 2012. Noncoding flavivirus RNA displays RNA interference suppressor activity in insect and Mammalian cells. *Journal of Virology* **86**: 13486–13500.

Schuessler A, Funk A, Lazear HM, Cooper DA, Torres S, Daffis S, Jha BK, Kumagai Y, Takeuchi O, Hertzog P *et al.* 2012. West Nile virus noncoding subgenomic RNA contributes to viral evasion of the type I interferon-mediated antiviral response. *Journal of Virology* **86**: 5708–5718.

Sola I, Almazán F, Zúñiga S, Enjuanes L. 2015. Continuous and discontinuous RNA synthesis in coronaviruses. *Annual Review of Virology* **2**: 265–288.

Sonenberg N, Hinnebusch AG. 2009. Regulation of translation initiation in eukaryotes: mechanisms and biological targets. *Cell* **136**: 731–745.

Steckelberg AL, Akiyama BM, Costantino DA, Sit TL, Nix JC, Kieft JS. 2018a. A folded viral noncoding RNA blocks host cell exoribonucleases through a conformationally dynamic RNA structure. *Proceedings of the National Academy of Sciences, USA* **115**: 6404–6409.

Steckelberg AL, Vicens Q, Kieft JS. 2018b. Exoribonuclease-resistant RNAs exist within both coding and noncoding subgenomic RNAs. *MBio* **9**: e02461-18.

Tamada T, Abe H. 1989. Evidence that Beet necrotic yellow vein virus RNA-4 is essential for efficient transmission by the fungus *Polymyxa betae*. *Journal of General Virology* **70**: 3391–3398.

Tamada T, Kusume T. 1991. Evidence that the 75K readthrough protein of beet necrotic yellow vein virus RNA-2 is essential for transmission by the fungus *Polymyxa betae*. *Journal of General Virology* **72**: 1497–1504.

Tamada T, Uchino H, Kusume T, Saito M. 1999. RNA 3 deletion mutants of beet necrotic yellow vein virus do not cause rhizomania disease in sugar beets. *Phytopathology* **89**: 1000–1006.

Varkonyi-Gasic E, Hellens RP. 2011. Quantitative stem-loop RT-PCR for detection of microRNAs. *Methods in Molecular Biology* **744**: 145–157.

van Vliet ALW, Smits SL, Rottier PJM, de Groot RJ. 2002. Discontinuous and non-discontinuous subgenomic RNA transcription in a nidovirus. *EMBO Journal* **21**: 6571–6580.

Wang Y, Fan H, Wang X-B, Li M, Han C, Li D, Yu J. 2011. Detection and characterization of spontaneous internal deletion mutants of Beet Necrotic yellow vein virus RNA3 from systemic host *Nicotiana benthamiana*. *Virology Journal* **8**: 335.

Zuker M. 2003. Mfold web server for nucleic acid folding and hybridization prediction. *Nucleic Acids Research* **31**: 3406–3415.

Supporting Information

Additional Supporting Information may be found online in the Supporting Information section at the end of the article.

Fig. S1 Complete sequence, translation and main features of beet soilborne mosaic virus chimeric RNAs.

Fig. S2 Quantification of the accumulation of beet soilborne mosaic virus genomic and chimeric RNAs by absolute RT-qPCR in upper systemically infected leaves of *Beta vulgaris* spp. *macrocarpa* and *Nicotiana benthamiana*.

Fig. S3 RT-PCRs performed on full-length *in vitro* generated beet soilborne mosaic virus (BSBMV) transcripts, transcripts of xrRNAs and on total RNA isolated from leaves infiltrated with BSBMV full-length infectious cDNA clones in the absence of RNA 1.

Fig. S4 Schematic representation of the representative RNA-Seq reads spanning the junction point (between RNA 2 and RNA3) in R2R3.

Fig. S5 Representative fluorescence microscopy images showing RFP-fluorescence in infection loci upon expression of RFP from R2R3 and R2R4, respectively.

Fig. S6 Complete sequence, translation and main features of the chimeric RNA species formed from beet soilborne mosaic virus RNA2 and BNYVV RNA3.

Fig. S7 Appearance of the symptoms in *Nicotiana benthamiana* induced by wt beet soilborne mosaic virus (BSBMV) and BSBMV mutants.

Fig. S8 Schematic representation of the stem-loop RT-qPCR principle developed in this study to quantify xrRNAs.

Fig. S9 A model for the synthesis of the minus strand on RNA3 and RNA4 templates involving interaction of 'coremin' with RNA2.

Table S1 List of primers used in this study.

Table S2 Stability of the mutations introduced into beet soilborne mosaic virus RNA2, RNA3 and RNA4.

Please note: Wiley is not responsible for the content or functionality of any Supporting Information supplied by the authors. Any queries (other than missing material) should be directed to the *New Phytologist* Central Office.